De-pollution efficacy of photocatalytic roofing granules

Xiaochen Tang[1], Lara Ughetta[2], Simon K. Shannon[2], Sébastien Houzé de l'Aulnoit[1], Sharon Chen[1], Rachael A. T. Gould[2], Marion L. Russell[1], Jiachen Zhang[3], George Ban-Weiss[3], Rebecca L. A. Everman[2], Frank W. Klink[2], Ronnen Levinson[1], Hugo Destaillats[1,*]

1. Heat Island Group, Lawrence Berkeley National Laboratory, 1 Cyclotron Road, Berkeley, California 94720, USA.
2. Industrial Mineral Products Division, The 3M Company, 3M Center, Building 209, 1-W-14, St. Paul, Minnesota 55144, USA.
3. Department of Civil and Environmental Engineering, University of Southern California, Los Angeles, California 90089, USA.

* Corresponding author E-mail: HDestaillats@lbl.gov

Keywords: asphalt roofing shingle, titanium dioxide, aging, weathering, NO_x, nitrate

Abstract

Photocatalytic building surfaces can harness sunlight to reduce urban air pollution. The NO_x abatement capacity of TiO_2-coated granules used in roofing products was evaluated for commercial product development. A laboratory test chamber and ancillary setup were built following conditions prescribed by ISO Standard 22197-1. It was validated by exposing reference P25-coated aluminum plates to a 3 L min^{-1} air flow enriched in 1 ppm NO under UVA irradiation (360 nm, 11.5 W m^{-2}). We characterized prototype granule-surfaced asphalt shingles and loose granules prepared with different TiO_2 loadings and post-treatment formulations. Tests performed at surface temperatures of 25 and 60 °C showed that NO_x abatement was more effective at the higher temperature. Preliminary tests explored the use of 1 ppm NO_2 and of 1 ppm and 0.3 ppm NO/NO_2 mixtures. Specimens were aged in a laboratory accelerated weathering apparatus, and by exposure to the outdoor environment over periods that included dry and rainy seasons. Laboratory aging led to higher NO removal and NO_2 formation rates, and the same catalyst activation was observed after field exposure with frequent precipitation. However, exposure during the dry season reduced the performance. This inactivation was mitigated by cleaning the surface of field-exposed specimens. Doubling the TiO_2 loading led to a 50–150 % increase in NO removal and NO_x deposition rates. Application of different post-treatment coatings decreased NO removal rates (21–35%) and NO_x deposition rates (26–74%) with respect to untreated granules. The mass balance of nitrogenated species was assessed by extracting granules after UV exposure in a 1 ppm NO-enriched atmosphere.

1. Introduction

Asphalt shingles are the most common residential roofing material in the US (about 80% market share) [1], while asphaltic built-up roofs and modified bitumen membranes are a popular option for low-pitch roofs on commercial buildings [2]. In both products, an impermeable asphaltic layer is surfaced with granules that impart durability and aesthetic properties. Photocatalytic roofing granules have the potential to provide additional environmental benefits by removing commonly found urban atmospheric pollutants such as nitrogen oxides (NO_x = NO + NO_2).

Under sunlight, photo-induced redox chemistry can eliminate soiling and air pollutants adsorbed on the catalyst surface, including organic compounds and atmospheric NO_x [3, 4]. Photocatalytic oxidation enables the removal of NO_x from urban air through their conversion to non-volatile byproducts following the oxidation sequence NO → NO_2^- / HNO_2 → NO_2 → NO_3^- / HNO_3 [5, 6]. The photocatalytic reaction of NO_x occurring at the TiO_2 surface is prompted by absorption of a UV-A photon (wavelength: 315-400 nm). The final stable oxidation byproducts can be washed off the surface by rain or dew. For that reason, emerging photocatalytic construction materials are specifically designed as *de-noxification* (*de-NO_x*) technologies. Several studies have explored in laboratory tests the initial performance of freshly prepared de-NO_x materials as a function of photocatalyst composition, allotropic form, porosity, microstructure, chemical interactions with substrates (e.g., cement, paint), relative humidity, water content, challenge gas composition, and catalyst loading [7-15]. Fewer studies report the de-NO_x performance of materials that had been aged in contact with the environment. For example, a recent study showed that a photocatalytic coating applied over concrete and plaster maintained about 80% of its initial activity after two years of continuous exposure to polluted urban air [16]. Similarly, a few large-scale field demonstrations of newly installed photocatalytic cementitious materials have been performed, showing disparate results ranging from excellent to poor de-NO_x efficacy [17-24]. The de-NO_x performance can change over time as materials are continuously exposed to the environment because photocatalytic efficacy is influenced by the buildup of recalcitrant residues on the surface (including microbial soiling) and by other physical and chemical changes associated with material aging. For that reason, it is important to evaluate the long-term performance of photocatalytic building materials in contact with the urban environment.

Various laboratory test methods have been developed to evaluate the air purification efficacy of photocatalytic materials [25-28]. A widely used approach is ISO Standard 22197-1: "Fine ceramics (advanced ceramics, advanced technical ceramics) – test method for air-purification performance of semiconducting photocatalytic materials. Part 1. Removal of nitric oxide" [29]. This popular method is convenient due to the simplicity of the test chamber and operation conditions, and allows for comparison across several products and materials that have been tested over the years using this standard. However, limitations and shortcomings have been identified, including possible underestimation of uptake rates due to slow diffusion from the gas phase to the catalyst [28, 30, 31]. An alternative methodology was proposed as an Italian (UNI) and European (CEN) standard, using a continuously stirred tank photo-reactor [28] to better address those biases. However, this approach may be affected by surface losses and gas-phase reactions due to longer residence times [31].

All standardized methods are designed to provide quantitative and reliable metrics to compare a wide range of materials. However, their results are not easily applicable to numerical models predicting the impacts on urban air quality of photocatalytic materials operating under real-world conditions. In these tests, photocatalysts are challenged with NO_x concentrations that exceed by one to two orders of magnitude the levels typically found in urban atmospheres (in the range 10 – 100 ppb); furthermore, in the case of ISO 22197-1, only NO is used as a reactant. The NO_x removal rate is calculated as the difference between consumed NO and formed NO_2, assuming that surface-bound nitrate is the only byproduct. However, it is possible that other byproducts besides HNO_3/NO_3^- could form during the photocatalytic process. In studies that explored byproduct formation in more detail, N_2O (a greenhouse gas) and nitrous acid (HONO, a reactive species) have been identified as relatively minor byproducts [32-36]. Another study found that HONO efficiently decomposed in contact with irradiated photocatalytic paint, and did not find N_2O [6]. Unlike nitrate, which can be effectively scrubbed from the atmosphere, HONO and N_2O may be re-emitted into urban air. Therefore, the mass balance of nitrogen-containing species should be considered to assess the environmental impact of these materials.

Another limitation of standardized methods is that they are run at ambient room temperature. Under the sunny summer afternoon conditions specified by ASTM Standard E1980-11: "Standard

practice for calculating reflectance index of horizontal and low-sloped opaque surfaces" [37], the surface temperature of a well-insulated roof with high thermal emittance (approximately 0.90) ranges from 45 °C if the solar reflectance is 0.80 (bright white color) to 83 °C for an albedo of 0.05 (black color). Two opposite effects can be expected to affect the photocatalytic performance at these relatively high roof temperatures, with respect to 25 °C: lower conversion rates due to poorer NO_x adsorption, and an acceleration of the processes due to faster reaction rates. There is little information regarding the effect of increasing surface temperature on the photocatalyzed oxidation of NO_x, and the evidence is not conclusive. One study described faster NO oxidation as temperature rose from 5 to 60 °C [38]. Another study showed that the NO_x removal rate decreased by increasing temperature from 30 °C to 40 °C at low relative humidity, but remained constant at a higher RH setting [39]. A third study observed a reduction in NO removal rates as temperature increased from 20 °C to 30 °C [8].

This study incorporates several factors to assess the performance of photocatalytic materials under realistic and standardized conditions. A modified version of the experimental approach from ISO 22197-1 was adopted to evaluate the photocatalytic performance of prototype granules used in asphalt shingles and modified bitumen roofing membranes. The effect of surface temperature was studied by operating the reactor at 25 °C (per ISO 22197-1) and 60 °C; the latter temperature represents a mid-range value corresponding to a roof albedo of 0.50 and a thermal emittance of 0.90. Tests were carried out mostly using 1,000 ppb NO as a challenge gas (per ISO 22197-1). Other conditions were also explored, that included the use of NO_2, an NO/NO_2 mixture, and lower upstream NO_x concentrations. Various granule formulations, which included different catalyst loading and post-treatments, were evaluated as received (unexposed), after accelerated aging in the laboratory, and after aging in the field. Surface-bound nitrate and nitrite were quantified, contributing to closing the mass balance for nitrogen-containing species.

2. Experiment

2.1 Materials

All tested photocatalytic materials were supplied by 3M, except for TiO_2–coated aluminum plates prepared at LBNL for use as reference samples. Two types of photocatalytic roofing materials

were tested: (1) loose granules with diameters of about 1 mm and varied surface coatings; and (2) prototype shingle samples prepared by adhering the granules to 10 cm × 20 cm aluminum plates coated with an acrylic layer. Both are illustrated in Figure S1 (Supporting Information). The loose granule samples were used to evaluate the role of different coating formulation parameters and to extract adsorbed species after irradiation. Shingles were used to expose the material to the natural environment and for accelerated aging in the laboratory. Three different groups of photocatalytic roofing materials (A, B, and C) were tested, as described in Table 1. All roofing granules comprised a base mineral core, a pigment coating and a photocatalyst coating. In addition, samples were coated with a proprietary adhesion promoter applied as a post-treatment to help granules stick to the asphalt shingle. Two post-treatment formulations were used, labeled PT1 and PT2, which were two variants of the standard method (STD) that included oil and silicone. Photocatalyst particles were TiO_2 Aeroxide® P25 (Evonik, Germany), except in one case in which TiO_2 Aeroxide® P90 (Evonik, Germany) was used in combination with P25 to evaluate the effect of incorporating a different catalyst. The catalyst was dispersed at either a low (1×) or high (2×) loading level through the silicate binder, and applied to the surface of the granules. The silicate binder formed a semi-ceramic coating at the surface of the granules after being fired at 200–370 °C. More details of the granule coating process are provided in two United States patents [40, 41].

Group A (shingles) included six different samples: a non-photocatalytic control sample (A0), shingles surfaced with granules prepared with three different types of photocatalytic coatings using the same base mineral and post-treatment PT1 (A1, A2 and A3), and two shingles using granules that incorporated a different post-treatment PT2 (A4 and A5). Multiple specimens were prepared and used for each shingle sample. The solar reflectance of the shingle prototypes ranged 0.12 – 0.30 (Table S1, Supporting Information). Group B (loose granules) included six types of white-pigmented samples with different P25 photocatalyst loading. These were further coated with two types of post-treatment formulations (PT1 and PT2), except in two cases that had not been post treated. Group C (loose granules) included four types of samples using a different base mineral, all with white-pigment coating and the same level of P25 photocatalyst coating. Varying levels of silicone in the post-treatment formulations was explored in this group to identify the optimal concentration of this additive. Three duplicate determinations were conducted with identical specimens, validating the consistency among samples and stability of the experimental method.

The reference samples were prepared by coating a 10 × 20 cm clean aluminum plate with different amounts of the P25 catalyst (20.0 mg for 1 g m^{-2} surface coverage and 200 mg for 10 g m^{-2}) suspended in 8 mL of de-ionized (DI) water. The suspension was pre-sonicated for 30 minutes to fully suspend the catalyst in water. After quantitatively transferring the suspension to the surface, the coated aluminum plate was heated at 60 °C, forming a homogeneous layer after water evaporated.

Table 1: Formulation of granule prototypes tested in this study.

Group	Sample	Color	TiO_2 P25 loading [a]	Post-treatment (PT) [b]
A (granule-surfaced shingles)	A0	White	No TiO_2 (control)	PT1
	A1	Grey	Low	PT1
	A2	Grey	High [c]	PT1
	A3	White	High	PT1
	A4	White	Low	PT2
	A5	White	High	PT2
B (loose granules)	B1	White	Low	None
	B2	White	High	None
	B3	White	Low	PT1
	B4	White	High	PT1
	B5	White	Low	PT2
	B6	White	High	PT2
C (loose granules)	C1	White	Low	PT1
	C2	White	Low	PT1 without silicone
	C3	White	Low	PT2
	C4	White	Low	Only STD

[a] In the range of 0.5 to 1.5 mg of catalyst per g of granules, per references #39 and #40.
[b] PT1 and PT2 are two modifications of a standard granule post-treatment using a proprietary composition (STD).
[c] Prepared using a P25 + P90 mixture

178 **2.2 Aging of shingle samples**

179 To evaluate potential changes in performance due to aging, shingle samples from Group A were
180 subjected to accelerated weathering in the laboratory and exposed to the environment (natural
181 aging) in two separate tests.

182 *2.2.1 Laboratory aging*

183 A sub-set of specimens from samples A1, A2, and A3 was exposed for 1,000 hours in a commercial
184 weathering apparatus (Model QUV/Spray with Solar Eye Irradiance Control, Q-Lab, Westlake OH)
185 following cycle 1 of ASTM Standard G154-12: "Standard practice for operating fluorescent
186 ultraviolet (UV) lamp apparatus for exposure of nonmetallic materials" [42]. This program
187 includes 8 h of ultraviolet (UV) irradiation (at 340 nm) with 0.89 W m^{-2} nm^{-1} intensity at 60 °C,
188 followed by 4 h water condensation at 50 °C. At 0.89 W m^{-2} nm^{-1}, the instrument delivers an hourly
189 irradiation of 275 kJ m^{-2}. Therefore, exposure in the QUV for 1,000 h is approximately equivalent
190 to 1 year of Florida sunshine (280 MJ m^{-2}) [43].

191 *2.2.2 Natural exposure*

192 Two separate natural aging exercises were performed on different sub-sets of A samples. In the
193 first case, shingle specimens corresponding to samples A1, A2 and A3 were exposed on racks
194 mounted on a laboratory roof in Berkeley, California (latitude 37.87° N, longitude 122.27° W).
195 Specimens were exposed for about 3 months during the spring and early summer of 2016 (2016-
196 03-25 to 2016-07-11), a dry period during which less than 10 mm of rain was recorded. The
197 maximum hourly average solar irradiance during this time period was 831 W m^{-2} (Table S3).
198 Meteorological data for the city of Berkeley was obtained from the nearby USC00040693 weather
199 station located at the UC Berkeley Campus (approximately 1 km west of the exposure site),
200 belonging to the Global Historical Climatology Network. Specimens for each sample were placed
201 in two south-facing racks tilted at a 45° angle with respect to the floor, as illustrated in Figure S2
202 (Supporting Information). At the end of the exposure period, specimens were retrieved, and their
203 NO_x removal efficacy was analyzed in the laboratory.

204 The second natural exposure test was carried out over a six month period with shingle samples A4
205 and A5, which were installed on 2017-01-13 in the racks tilted at 45° with respect to the horizon.
206 Several identical specimens of each sample were installed side by side and retrieved at different

times. Those retrieved on 2017-04-26, after three months of exposure, experienced a rainy winter and early spring, with a total precipitation of 308 mm during that period. By contrast, specimens withdrawn after six months of exposure, on 2017-07-11, had been subsequently exposed to significantly less additional rain (66 mm), which occurred only in the month of April. The cumulative precipitation during the six-month period is presented in Figure S3 (Supporting Information). Average solar irradiance is reported in Table S2 (Supporting Info.). The solar irradiance was weaker in this 6-month period, with a maximum hourly average value of 559 W m^{-2} (Table S3). Specimens retrieved at 3 and 6 months were analyzed in the laboratory to evaluate their NO_x removal efficacy.

After determining their de-NO_x performance, specimens retrieved at 6 months were subsequently cleaned in the lab and re-analyzed to assess their regeneration potential. Two cleaning methods were used. In the first ("soft cleaning") the shingle surface was rinsed four times with 25 mL of de-ionized water using a squirt bottle. In the "hard cleaning" process, the specimen was placed in a beaker filled with de-ionized water and sonicated for 60 min, to facilitate contact between water and occluded materials. Both cleaning operations are illustrated in Figure S4 (Supporting Information).

2.3 Evaluation of the photocatalytic performance

2.3.1 Experimental setup

A bench-scale exposure apparatus and ancillary system was built following conditions stipulated by ISO Standard 22197-1 [29]. The exposure chamber consisted of a flow reactor, UV irradiation source and temperature control using a thermostatic water bath, as illustrated in Figure 1. In each test, a rectangular specimen of 10 × 20 cm was placed flat at the bottom of the chamber where a quartz window admitted ultraviolet lamplight. The gap between the sample and the window was 5 mm. Air enriched with a target concentration of 1,000 ppb NO was introduced upstream at 50% relative humidity (RH) by diluting a 50 ppm NO flow from a pre-mixed cylinder (Praxair, Danbury, CT). In experiments using NO_2 as a challenge gas (by itself or in mixtures with NO), a pre-mixed NO_2 cylinder of 50 ppm was used (Praxair, Danbury, CT). In experiments using upstream concentrations lower than 1,000 ppb, those levels were achieved by reducing the flow delivered

by the NO and NO_2 cylinders. Downstream of the system, a chemiluminescent NO_x analyzer (Model 200A, Teledyne Technologies, Thousand Oaks, CA) was used to record in real time the concentrations of NO and NO_2 present in the air at the chamber's outlet. The NO_x analyzer was calibrated at different times during the tests. Three duplicate determinations were conducted with identical specimens, validating the consistency among samples and stability of the experimental method.

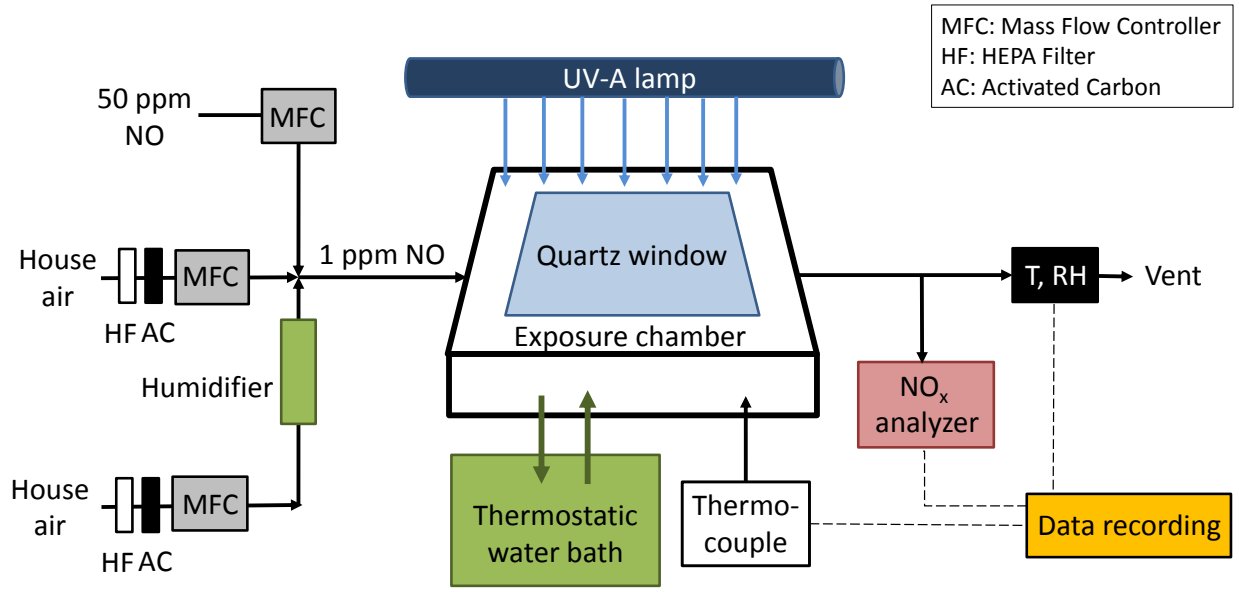

Figure 1: Experimental setup following the ISO 22197-1 method with temperature controlling function.

Experiments were carried out at room temperature (per ISO 22197-1) and also at a higher temperature by heating the sample to 60 °C, simulating typical roof temperatures. For the high-temperature experiments, the chamber base temperature was regulated by circulation of water from a thermostatic bath using copper tubing embedded in the bottom of chamber. The chamber base temperature was measured with an inserted thermocouple in good contact with it. Due to its relatively short residence time (approximately 2 s), the NO-enriched air flowing through the apparatus was not heated and remained at room temperature. The temperature and relative

humidity (RH) of the air exiting the chamber was monitored with an in-line digital T/RH sensor (HIH6100 series, Honeywell, Morris Plains, NJ) and recorded in real time. The RH was controlled by splitting the dilution upstream flow, saturating air in one of the lines by circulation through a water bubbler, and adjusting the relative flow ratios while keeping the total flow rate at 3 L min^{-1}.

Constant UV irradiation at 360 nm (UVA) was provided by a 15 W mercury fluorescent lamp (Model TL-D, Actinic BL, Philips, Andover, MA). The UV irradiance at 360 nm wavelength was measured at different points on the specimen's surface with a digital radiometer (Model UVX, UVP LLC, Upland, CA). The irradiance was highest at the center of the sample and consistent over the exposed surface, with an average of 11.5 ± 1.5 W m^{-2}. Irradiance measurements were performed prior to the beginning of tests and repeated at the end, confirming consistency of the lamp output over the experimental period.

2.3.2 NO_x removal rate and predicted nitrate buildup rate

Each individual test comprised three periods in the test chamber:

a) pre-equilibration of the specimen in the dark with a constant flow of the NO-enriched air;

b) 4 – 6 h (usually 5 – 6 h) of continuous UV illumination under a constant flow of the NO-enriched air; and

c) a final dark period of about 1 h with a constant flow of the NO-enriched air, to verify restoration of the initial NO levels.

Most of the NO reacted in the first 2-3 hours of irradiation, and the phenomenon was fully captured with a minimum UV exposure of 4 hours. In most tests the irradiation period was 6 hours. The calculation of NO and NO_2 reaction rates considered the total length of irradiation time. NO removal rate (r_{NO}, μmol h^{-1}) and NO_2 formation rate (r_{NO_2}, μmol h^{-1}, from oxidation of NO) were calculated using the difference between the inlet and outlet concentrations of NO and NO_2:

$$r_{\mathrm{NO}} = \frac{\int_0^{\tau} n_{\mathrm{NO_{removed}}}(t)\, dt}{\tau} = \frac{\int_0^{\tau} [c_{\mathrm{NO_{in}}}(t) - c_{\mathrm{NO_{out}}}(t)] dt}{\tau} \times \frac{Q}{V_{\mathrm{n}}} \qquad (1)$$

$$r_{NO_2} = \frac{\int_0^{\tau} n_{NO_{2formed}}(t)\,dt}{\tau} = \frac{\int_0^{\tau}[c_{NO_{2out}}(t) - c_{NO_{2in}}(t)]\,dt}{\tau} \times \frac{Q}{V_n} \quad (2)$$

where Q is the air flow rate (L min^{-1}), τ is duration of irradiation (h), t is time (min), n is the number of moles (mol), c is the concentration in the air (μmol m^{-3}), and V_n is the normalized gas volume for one mole of gas at standard pressure and room temperature (22.4 L). The predicted maximum nitrate formation rate from oxidation of NO and NO_2 ($r_{nitrate}$, μmol h^{-1}) was determined from a mass balance, assuming that nitrate and NO_2 are the only byproducts of NO oxidation:

$$r_{nitrate} = r_{NO} - r_{NO_2} \quad (3)$$

This approach provides best-case scenario predictions of the amount of nitrate that can be formed in the process. The relative yield of NO_2 (Y_{NO_2}) and predicted nitrate yield ($Y_{nitrate}$) can be determined as the ratio between their formation rates and the NO reaction rate, as follows:

$$Y_{NO_2} = \frac{r_{NO_2}}{r_{NO}} \quad (4)$$

$$Y_{nitrate} = \frac{r_{nitrate}}{r_{NO}} \quad (5)$$

Since these are the only two byproducts considered in the analysis, $Y_{NO_2} + Y_{nitrate} = 100\%$. The predicted maximum nitrate buildup rate is reported as the mass of nitrate formed per unit time and area (in mg h^{-1} m^{-2}), and the NO_x deposition rate (D_{NO_x}) is calculated as the difference between NO removal and NO_2 formation rates per unit area (Eq. 6), expressed in moles (in μmol h^{-1} m^{-2}):

$$D_{NO_X} = \frac{r_{NO} - r_{NO_2}}{A} \quad (6)$$

in which A is the exposed surface area, equal to 0.02 m² in all tests. In each experiment, NO loss rate (r_{NO}), NO_2 formation rate (r_{NO_2}), relative yield of NO_2 (Y_{NO_2}) and NO_x deposition rate (D_{NO_x}) was calculated following Eqs. (1), (2), (4) and (6), respectively.

2.3.3 Extraction and analysis of adsorbed nitrogenated byproducts

After being tested in a regular experiment in which NO-enriched air was flown through the reactor and the sample was irradiated over 6 hours, 5.0 g of the loose granules was extracted in water (ion chromatography grade, Sigma Aldrich) by sonication for 30 minutes. The supernatant was left for at least 48 hours in contact with the granules prior to filtration using 0.22 µm pore size syringe filter (Millipore). Another two successive extractions of the same granules were conducted to ensure the maximum amounts of nitrate (NO_3^-) and nitrite (NO_2^-) ions were eluted from the granules. Between each extraction, the supernatant was transferred to a separate volumetric container, and its volume was recorded. The total amount of anion mass detected in the sum of all three extractions was calculated. There was a significant experimental error associated with this method, in the order of 20% (5% from NO_x measurement, 10% from supernatant volume readings, and 5% from distribution of nitrate on granule surfaces).

Extracts were analyzed by a Dionex Ion Chromatography System (ICS), model 2000. The ICS is equipped with an autosampler (AS40, Dionex), a hydroxide ion generator (EluGen cartridge, Dionex), a conductivity detector, and an ASRS 300 suppressor. Samples were separated isocratically on an AS11-HC column (Dionex) at 20 mM hydroxide ion and a flow rate of 1.0 mL min^{-1} at 30 °C. An injection loop of 25 µL was used to inject samples. A multi-point calibration ranging from 0.1 mg L^{-1} to 10.0 mg L^{-1} was prepared by diluting a 1.000 g L^{-1} nitrite and nitrate chromatography standard (Sigma Aldrich) and was used to quantify the instrument response. A typical calibration curve has a relative standard deviation of 1.9% and a coefficient of determination of 0.9998. Nitrate and nitrite were quantified in extracts from granules that had been used in the chamber with NO-enriched air. Unexposed granules were also extracted to determine background (blank) values.

3. Results and Discussion

3.1 Validation using a reference photocatalytic sample

Prior to carrying out experiments using prototype granules or shingles, the approach was validated by performing tests on P25-coated aluminum plates. The removal rate of NO, formation rate of NO_2, NO_2 yield, NO_x deposition rate and the predicted rate of nitrate buildup were calculated in two separate tests at room temperature using different values of P25 surface coverage, and are reported in Table 2. Figure 2 presents results corresponding to tests using P25 surface coverage of 1 g m^{-2} (Figure 2-A) and 10 g m^{-2} (Figure 2-B). Overall, the NO_x deposition rate and the predicted nitrate buildup rate increased with the catalyst surface coverage, suggesting that the photocatalytic process is limited by the number of available reaction sites. NO_x deposition rates were 18 and 296 µmol h^{-1} m^{-2} for P25 surface coverage values of 1 and 10 g m^{-2}, respectively. These results are consistent with a value of 192 µmol h^{-1} m^{-2} determined using 5 g m^{-2} P25 by Mills and Elouali following the same ISO method [30].

Table 2: Summary of results for P25-coated reference samples and Group A shingle samples.

Surface temperature, challenge gas	Sample	UV treatment (h)	NO loss rate, r_{NO} (µmol/h)	NO_2 formation rate, r_{NO_2} (µmol/h)	Relative NO_2 yield, Y_{NO_2} (%)	NO_x deposition rate (µmol/h·m^2)	Predicted maximum nitrate buildup rate (mg/h·m^2)
P25-coated reference samples							
25 °C 1,000 ppb NO	1 g/m^2	6.0	4.0	3.7	91	18 ±1	1.1 ± 0.1
	10 g/m^2	5.6	8.3	2.4	29	296 ±2	18 ± 0.1
25 °C 1,000 ppb NO_2	1 g/m^2	6.0	-0.07	-1.3	n.a.	62 ± 1	3.8 ± 0.5
60 °C 1,000 ppb NO	1 g/m^2	6.0	5.2	3.7	72	73 ±2	4.5 ±0.5
60 °C 1,500 ppb NO_2	1 g/m^2	6.0	-0.4	-1.3	n.a.	47 ±1	2.9 ±0.1
60 °C 1,000 ppb NO/NO_2	1 g/m^2	6.0	0.96	0.13	n.a.	41±2	2.6 ±0.1
60 °C 300 ppb NO/NO_2	1 g/m^2	6.0	0.3	-0.1	n.a	21±1	1.3 ±0.03
Unexposed samples							
25 °C 1,000 ppb NO	A1	4.6	0.09	n.d.	n.d.	4.5 ±0.9	0.28 ±0.06
	A2	5.0	0.91	0.43	47	24 ±4	1.5 ±0.2
	A3	4.3	0.19	0.04	22	7 ±2	0.5 ±0.1
60 °C 1,000 ppb NO	A1	5.3	0.08	0.03	36	2.4 ±1.1	0.15 ±0.07
	A2	5.5	2.9	1.3	45	80 ±6	5.0 ±0.4
	A3	5.2	0.28	0.07	24	11 ±1	0.67 ±0.09
	A4	6	0.095	0.062	65	1.6 ±1.0	0.10 ±0.06
	A5	6	0.17	0.071	43	4.7 ±0.8	0.29 ±0.05
Samples exposed to 1000-hour laboratory accelerated aging							
60 °C 1,000 ppb NO	A1	5.3	0.15	0.11	72	2 ±2	0.1 ±0.1
	A2	6.0	2.6	2.2	84	21 ±3	1.3 ±0.2
	A3	6.0	1.7	1.5	87	11 ±1	0.7 ±0.1
Samples exposed to 3 months of natural aging @ 45° tilt angle (2016-03-25 to 2016-07-11)							
60 °C 1000 ppb NO	A1	6.0	0.06	n.d.	n.d.	3 ±2	0.2 ±0.1
	A2	6.0	1.6	1.2	72	23 ±1	1.4 ±0.1
	A3	6.0	0.41	0.28	69	6.3 ±1.3	0.4 ±0.1
Samples exposed to 3 months of natural aging @ 45° tilt angle (2017-01-13 to 2017-04-26)							
60 °C 1,000 ppb NO	A4	6.0	0.73	0.49	67	12 ±2	0.75 ±0.09
	A5	6.0	1.41	1.03	73	19 ±2	1.2 ±0.09
Samples exposed to 6 months of natural aging @ 45° tilt angle (2017-01-13 to 2017-07-11)							
60 °C 1,000 ppb NO	A4	6.0	0.30	0.22	73	4 ±1	0.26 ±0.07
	A5	6.0	0.65	0.52	80	6.7 ±0.6	0.41 ±0.04
Samples cleaned after 6 months of natural aging @ 45° tilt angle							
60 °C 1,000 ppb NO	A4 – soft	6.0	0.24	0.15	64	4.4 ±0.7	0.27 ±0.05
	A4 – hard	6.0	0.38	0.29	78	5 ±1	0.26 ±0.07
	A5 – soft	6.0	0.54	0.33	60	11 ±1	0.68 ±0.09
	A5 - hard	6.0	0.94	0.72	77	12 ±1	0.68 ±0.09

n.a..: does not apply (NO_2 is the reactant); n.d.: not detected

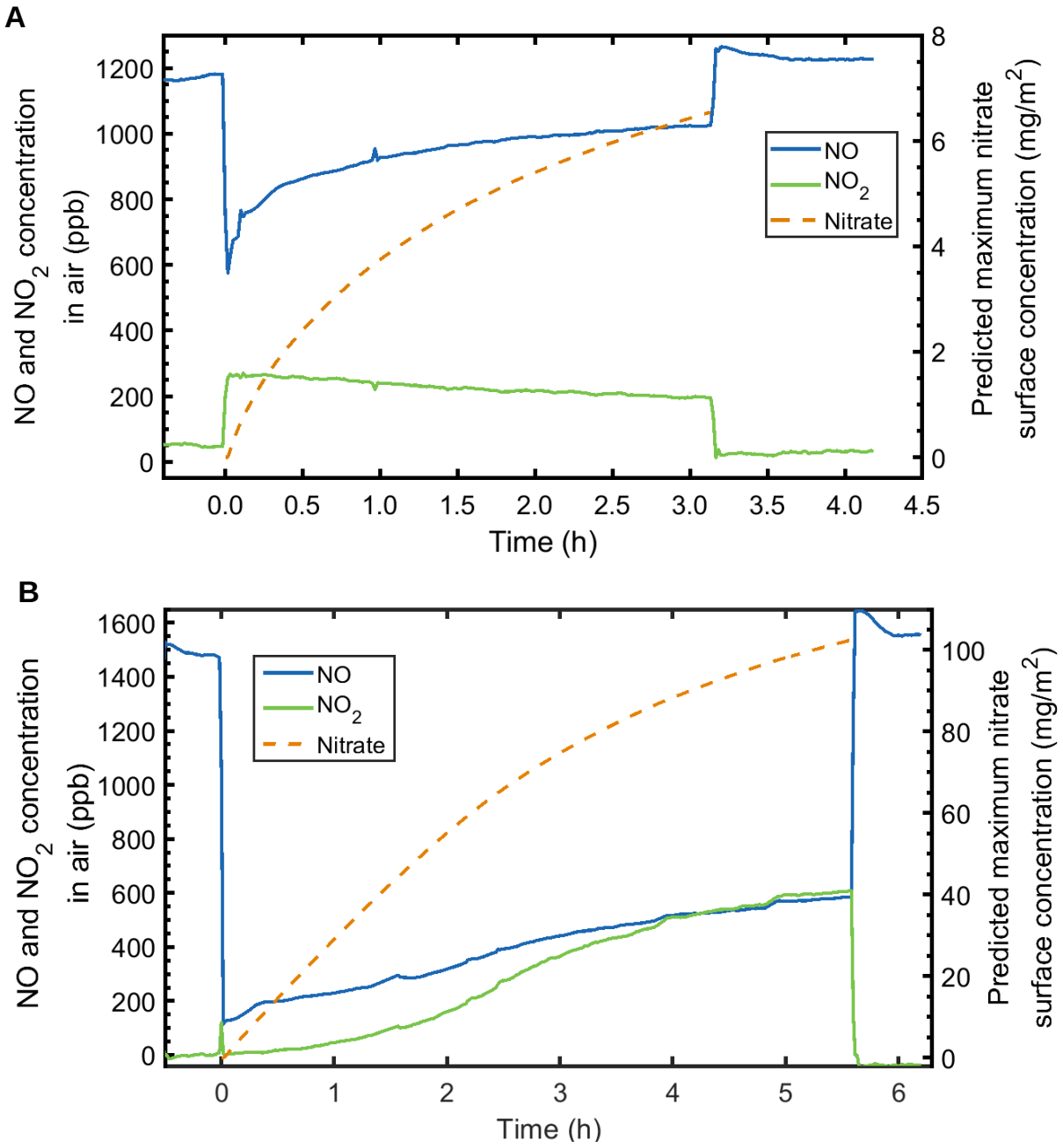

340
341
342 **Figure 2**: Evolution of NO and NO_2 concentrations during UV irradiation of an aluminum plate
343 coated with **(**A**)** 1 g/m² or **(**B**)** 10 g/m² of Aeroxide® P25 TiO_2**.** The predicted maximum
344 concentration of adsorbed nitrate (dashed curve) is reported on the right y-axis.
345

3.2 Influence of specimen temperature on de-NO_x efficacy

P25 reference (1 g m^{-2}) samples and unexposed Group A shingles were tested separately at both 25 °C and 60 °C, with all the other experimental parameters remaining the same. Results are presented in Table 2. Curves obtained for shingle sample A2 at both temperatures are shown in Figure 3. Tests carried out at 60 °C showed higher rates for NO oxidation, NO_x deposition and predicted nitrate buildup for the P25 reference sample and for two of the three tested shingle samples with respect to measurements carried out at room temperature. The P25 reference sample had a predicted NO_x deposition rate that was 4 times higher at 60 °C than at 25 °C, while the same parameter for samples A2 and A3 was 3.3 and 1.5 times higher, respectively, at 60 °C than at 25 °C. These results suggest that increasing the surface temperature led to faster photocatalytic reactions, an outcome favorable to the depollution process. Based on these results, it was decided to perform the tests corresponding to sample Groups B and C at 60 °C, better simulating conditions relevant for roofing materials under the sun.

These temperature effects can be viewed in the context of a few other studies reporting also the effect of surface temperature on the photocatalytic performance. A study of concrete pavements shows a positive correlation between NO oxidation rates and temperature, with rates tripling as temperature increased from 5 to 60 °C [38]. This result is consistent with the trends reported here. However, a study of photocatalytic stucco coatings found that the NO_x removal rate decreased by increasing temperature from 30 °C to 40 °C when the relative humidity was low (20%), and remained constant for a higher relative humidity of 65%, suggesting that other factors—such as competition for surface sites with moisture and the nature of the substrate—may play a significant role [39]. A study of photocatalytic mortar also showed that increasing temperature from 20 °C to 30 °C led to a reduced removal rate for NO [8]. Hence, our results and the limited literature available on the subject suggest that other environmental factors and the nature of the surfaces may affect the temperature dependence of NO_x photocatalytic oxidation. These apparent contradictions should be clarified when more research becomes available.

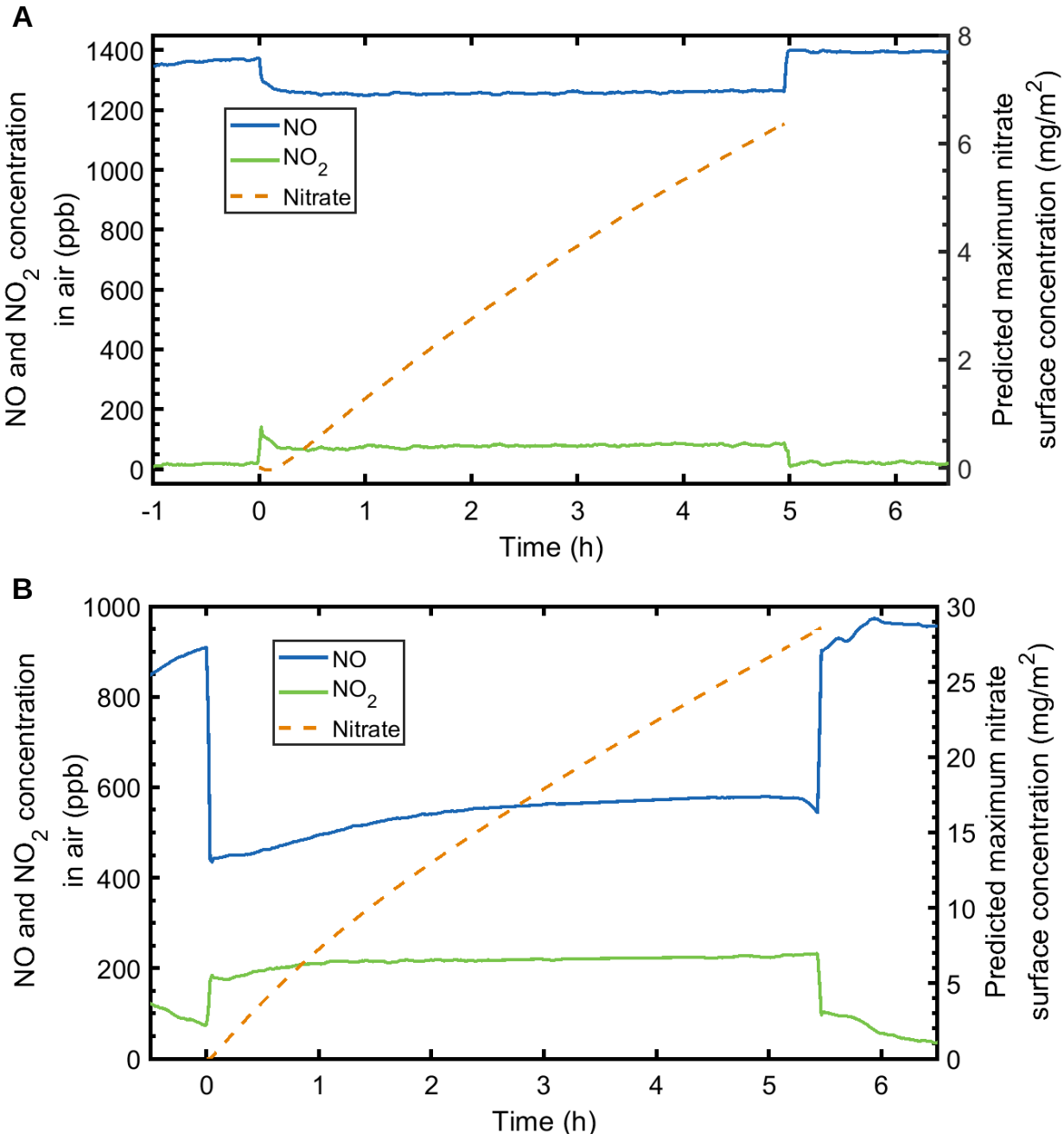

373

374 **Figure 3**: Evolution of NO and NO_2 concentrations during UV irradiation of an unexposed
375 shingle Sample A2 at **(**A**)** room temperature; **(**B**)** 60 °C. The predicted maximum concentration
376 of adsorbed nitrate (dashed curve) is reported on the right y-axis.

377

378

3.3 Using NO, NO_2 and NO/NO_2 mixtures as challenge gas

In ISO Standard 22197-1, air enriched with 1,000 ppb NO is used to challenge the photocatalytic surface. The same conditions were used in this study. However, in preliminary work we also explored the alternative use of NO_2 and a mixture with a 0.3 NO/NO_2 ratio. The latter is a mixing ratio commonly found in urban air in Los Angeles (see Figure S5 and Table S3, Supporting Information). These additional tests were carried out using P25-coated aluminum plates with 1 g m^{-2} catalyst, and results are reported in Table 2. NO_2 was tested at 25 °C (1,000 ppb) and 60 °C (1,500 ppb), while the NO/NO_2 mixture was tested at 60 °C for two total NO_x concentrations of 1,000 ppb and 300 ppb. Experimental traces corresponding to these tests are shown in Figure 4. The corresponding formation and removal rates for NO and NO_2, and the NO_x deposition rates, are presented in Figure 5. The difference in removal and formation rates for NO and NO_2 at each temperature determined the extent of NO_x deposition.

De-NO_x efficiency of the P25 reference sample was influenced by the challenge gas species and reaction temperature. At 25 °C, the use of NO_2 increased the NO_x deposition rate by a factor of >3, compared with experiments in which the catalyst was exposed to NO. However, the opposite trend was observed at 60 °C: using NO as a challenge gas resulted in a higher NO_x deposition rate than with NO_2. When NO_2 was used as the single challenge gas or as a principal component of the NO/NO_2 mixture, its concentration dropped rapidly during the first few minutes of UV irradiation, consistent with its higher affinity for the TiO_2 surface than that of NO [14, 44]. This initial uptake of NO_2 was followed by a rapid recovery in downstream NO_2 concentration during the initial hour (Figure 4). This behavior is qualitatively different from that observed for NO (Figure 3) and suggests that NO_2 oxidation led primarily to the formation of adsorbed species that partially inactivated the catalyst. When pure NO_2 was used as challenge gas, NO formation was observed, indicating that other chemical processes were taking place in addition to the photooxidation reaction. Those reactions likely involved disproportionation of NO_2 and/or photoreduction of adsorbed nitrate [45-47]. When the NO/NO_2 mixture was used, the final NO_2 concentration at the end of the 6 h irradiation period was higher than the upstream concentration (Figures 4B and 4C), suggesting that a net conversion of NO into NO_2 exceeded the amount of NO_2 being eliminated at the end of the irradiation period. Tests carried out at 300 ppb NO/NO_2 mixture showed a

proportionally lower NO_x deposition rate than those performed at 1,000 ppb (21 vs. 41 µmol h^{-1} m^{-2}, respectively).

In summary, using different challenge gas had a large effect in the chemical process, the net removal and formation of NO and NO_2, and the NO_x deposition rate. It should be kept in mind that these reaction rates are integrated for 6 h periods during which the relative elimination and formation rates of NO and NO_2 are not constant, further adding to the complexity of this analysis. For that reason, normalized test conditions such as those used in ISO 22197-1 are necessary to provide a meaningful metric.

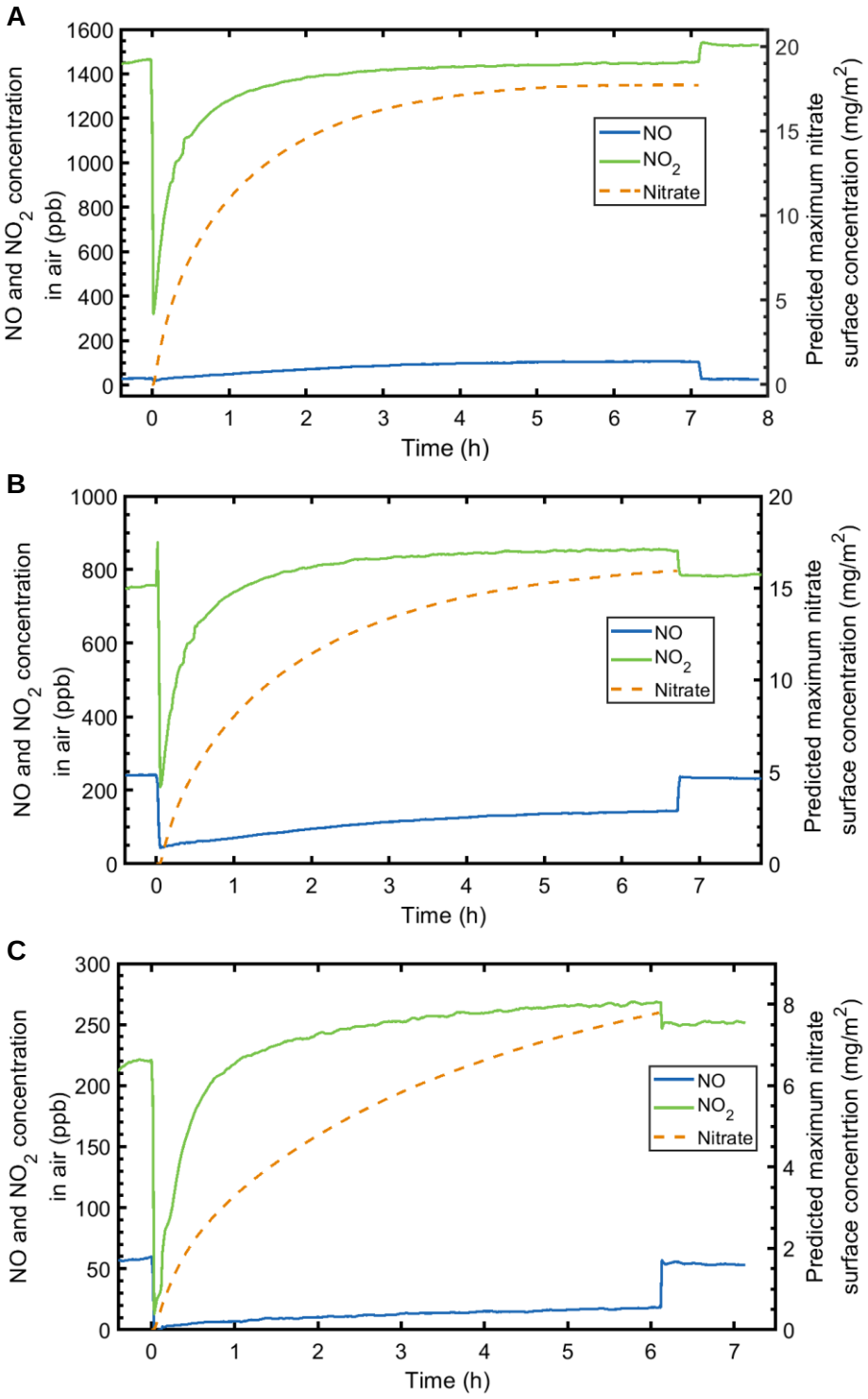

Figure 4. Experimental traces corresponding to experiments using a P25-coated plated (1 g m^{-2}) at 60 °C challenged with (A) NO_2, 1000 ppb; (B) NO/NO_2 = 0.3, 1000 ppb; (C) NO/NO_2 = 0.3, 300 ppb.

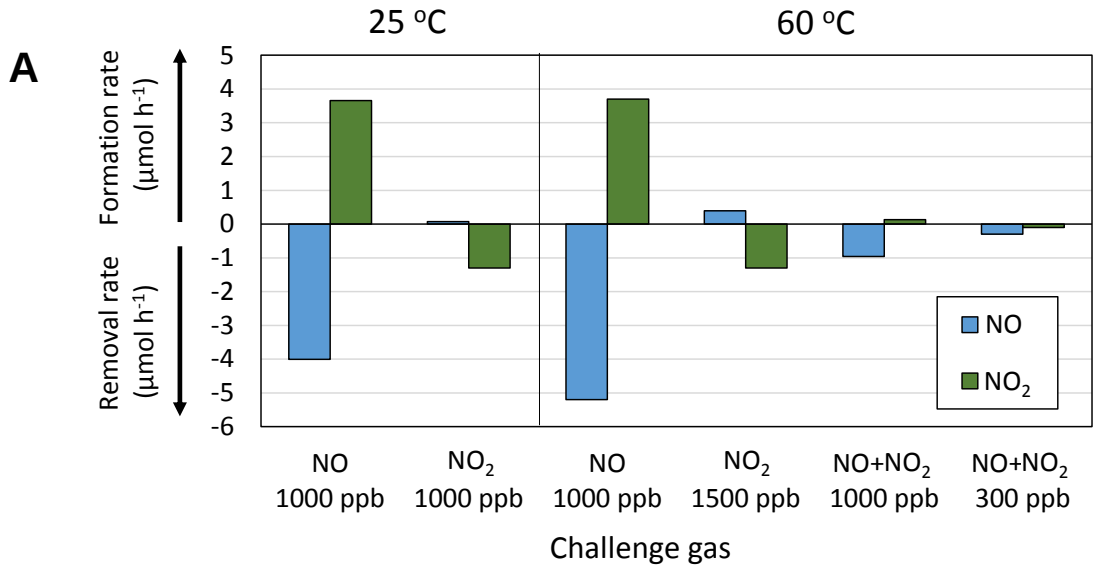

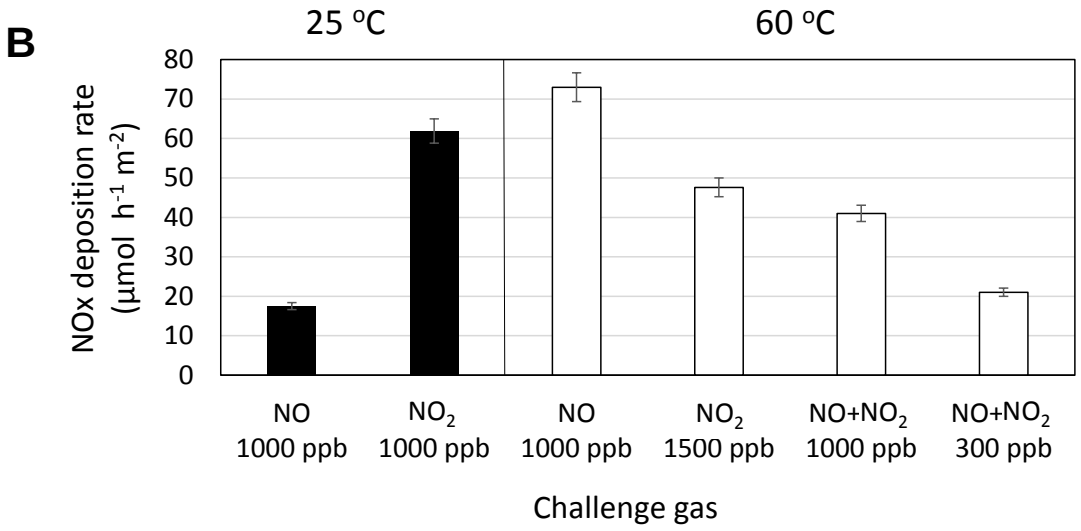

Figure 5: Use of different challenge gases to assess the performance of a reference 1 g/m² P25 sample, by measuring **(**A**)** removal and formation rates for NO and NO_2; **(**B**)** NO_x deposition rate.

3.4 Influence of material aging on de-NO_x efficacy

The results for the fresh (unexposed) and aged samples corresponding to Group A are summarized in Table 2. In all cases, the performance was evaluated with a 1,000 ppm NO challenge, at 60 °C. Figures 6 and 7 show the reaction rates and relative yield of NO_2 and nitrate formation for the unexposed materials and for shingles aged under different conditions. Both laboratory aging and field exposure were found to induce changes in the photocatalytic activity of the shingle samples, reflected in variations not only of the NO and NO_2 reaction rate, but also of the NO_x deposition rate and the predicted maximum nitrate buildup rate.

3.4.1 Laboratory aging

Exposure of specimens in the laboratory weathering apparatus led, in most cases, to an increase in NO removal and NO_2 formation rates, as compared with unexposed samples. Such activation of the photocatalyst did not necessarily translate into higher NO_x deposition rates, because most of the additional NO consumed was converted into NO_2, with a net zero NO_x balance (Figure 6).

3.4.2 Field exposure

Two sets of shingles were exposed in the field during different periods. In the first case, three months of natural aging reduced the photocatalytic activity of samples A1 and A2, but sample A3 was not influenced by aging. The NO_x removal efficiency was reduced for all three samples (Figure 6). This result is consistent with catalyst inactivation and partial blockage of active sites by particulate matter and other atmospheric chemicals deposited on the surface. It should be noted that the exposure period was fully within the dry season in Northern California. The lack of precipitation likely contributed to soiling buildup and catalyst inactivation.

By contrast, the second set of shingles (A4 and A5) was exposed during the rainy season during the initial three months, followed by another three months capturing the dry season (Figure 7). Both samples were strongly activated during the rainy season, and the activity decreased after the second period. The NO_x deposition rate increased significantly during the rainy season, but it dropped back to levels similar to those recorded for the unexposed samples at the end of the six-month period. Specimens that were exposed for six months were subsequently cleaned in the laboratory using two different protocols. A simple rinsing of the surface (“soft cleaning”) slightly reduced both the NO removal and NO_2 formation rates but increased the NO_x deposition rates for

samples A4 and A5 by 10% and 64%, respectively. The more energetic ("hard") cleaning using an ultrasonic bath led to higher NO and NO_2 rates, also with a higher NO_x deposition rate in the case of samples A4 (25%) and A5 (79%). The changes observed during dry and rainy periods, and the partial recovery of the activity due to surface cleaning, support the hypothesis that the accumulation of surface species partially blocking the catalyst can be mitigated by dissolution of water-soluble species (including nitrate), combined with physical removal. This observation is consistent with that of Lettieri et al. [24] showing that photodegradation efficiency of TiO_2-coated limestone decreased after eight months of exposure in the field, which was partially recovered after washing the sample surface with water. The deactivation of TiO_2 catalyst may be caused by the loss of TiO_2 nanoparticles, as well as blockage of active photocatalytic sites as a result of contaminant degradation intermediates and byproducts [48].

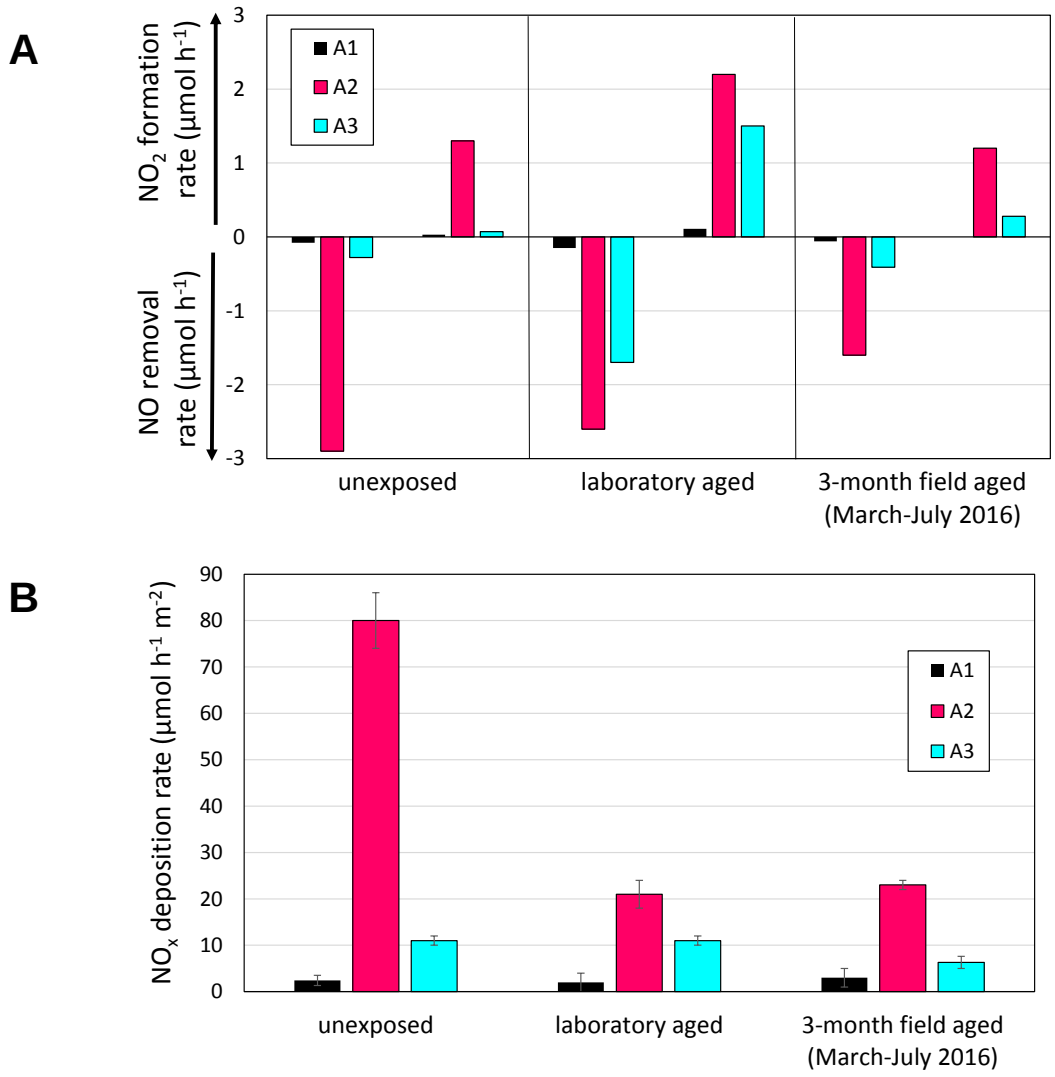

Figure 6: Comparison of (A) reaction rates and (B) NO_x deposition rates determined for three shingle samples prior to exposure, after laboratory aging and after three months of exposure in the field during the dry season. Tests were carried out with a challenge of 1,000 ppb NO at 60 ºC.

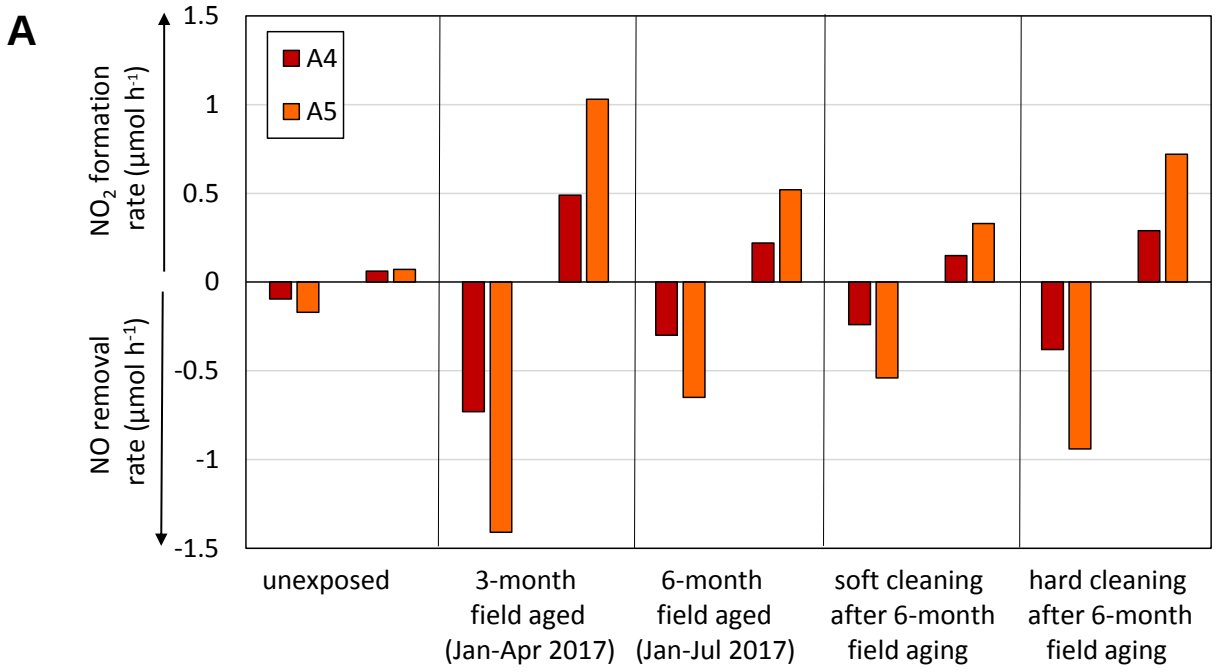

474

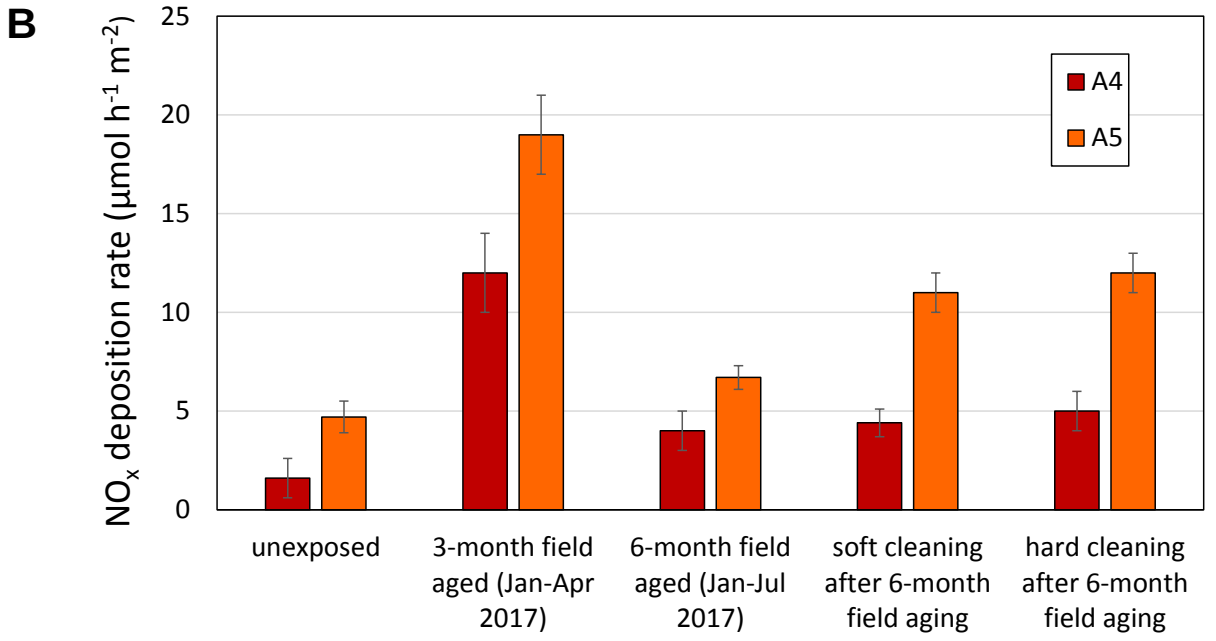

475

476 **Figure 7:** Comparison of (A) reaction rates and (B) NO_x deposition rates determined for two
477 shingle samples under different conditions. Tests were carried out with a challenge of 1000 ppb
478 NO at 60 ^{o}C.

3.5 Influence of granule coating formulations

Photocatalyst loading and the application of different post treatment coatings influenced the de-polluting capabilities of shingle and loose granule samples. Shingles with more photocatalyst outperformed corresponding samples with the same post-treatment and a lower P25 loading (e.g., A3 > A1 and A5 > A4). In the case of sample A2, the presence of a different type of catalyst (P90) in combination with P25 led to increased activity. The non-photocatalytic control sample A0 showed no de-NO_x activity.

The combined effect of the photocatalyst loading and different post treatments was further examined with Group B granule samples (Table 3). While the irradiation duration for samples B2 and B3 was different than that for B1, most NO reacted in the first 2-3 h, thus the illumination duration did not have a major impact on the determined parameters. Samples with the higher photocatalyst loading per mass of granule showed higher NO_x removal capacity than those with a lower loading. Similar to the above described results for Group A, doubling the photocatalyst loading led to a proportional increase of 50–100 % in the NO reaction rate and the NO_x deposition rates. Comparing granules with the same photocatalyst loading, those with PT1 (B3) and PT2 (B5) showed lower performance than a similar sample without post-treatment (B1). Comparing samples with the lower P25 loading, the NO removal rates were 14% (B3) and 6% (B4) of the value determined for B1. Similarly, for the same samples the NO_x deposition rate was 28% (B3) and 6% (B5) with respect to B1. The same analysis applied to samples with the higher P25 loading showed that NO removal rates for post-treated samples were 12% (B4) and 5% (B6) the value corresponding to B2, and the NO_x deposition rates were 26% (B4) and 8% (B6) those of B2.

The potential influence of silicone used in post-treatment formulations was evaluated with Group C loose granules (Table 3). While the potential deactivation of TiO_2 active sites by siloxanes is well documented [49, 50], there was no significant reduction in the photocatalytic activity caused by the presence of silicone. The differences observed are of the same magnitude as the experimental error; additional studies will be needed to better assess the role of silicone.

Table 3: Experimental results for Group B and Group C loose granule samples.

Challenge NO concentration (ppb)	Sample	TiO_2 P25 loading	Post treat-ment [a]	UV treatment (h)	NO loss rate, r_{NO} (μmol/h)	NO_2 formation rate, r_{NO_2} (μmol/h)	Relative NO_2 yield, Y_{NO_2} (%)	NOx deposition rate (μmol/h·m²)	Predicted maximum nitrate buildup rate (mg/h·m²)
1,000	B1	Low	–	6	1.8	1.2	68	29 ±1	1.8 ±0.1
1,000	B2	High	–	4.4	3.3	2.1	65	58 ±2	3.6 ±0.2
760[b]	B3	Low	PT1	5.1	0.25	0.09	35	8.0 ±0.6	0.50 ±0.04
1,000	B4	High	PT1	6	0.41	0.11	26	15 ±1	0.93 ±0.05
1000	B5[c]	Low	PT2	6	0.10	0.06	65	1.6 ±1.0	0.1 ±0.06
1000	B6[c]	High	PT2	6	0.17	0.07	43	4.7 ±0.8	0.29 ±0.05
1,000	C1	Low	PT1	6	1.7	0.43	25	65 ±19	4.1 ±1.2
1,000	C2	Low	PT1 w/o silicone	6	1.5	0.33	22	59 ±8.2	3.6 ±0.5
1,000	C3	Low	PT2	6	1.4	0.36	26	52 ±6.6	3.2 ±0.4
1,000	C4	Low	Only STD	6	1.9	0.41	22	72 ±5.9	4.5 ±0.4

[a] PT1 and PT2 are two modifications of a standard granule post-treatment using a proprietary composition (STD).
[b] Slightly lower challenge NO concentration was used due to lower MFC setting.
[c] Shingle sample instead of loose granule sample was used in the experiment.

3.6 Mass balance of nitrogenated species

In the experiments reported in Tables 2 and 3, the calculation of maximum nitrate buildup rate assumed that no other nitrogenated species were formed and that nitrate anions remained on the surface. This hypothesis was evaluated by extracting four different loose granule samples from Group C that had previously been exposed to NO-enriched air as described in Section 2.3.3. Unexposed granules from the same samples were also extracted, as a reference. The mass of nitrate and nitrite anions determined for each sample (in duplicate determinations) is reported in Figure 8. These values were determined from the sum of three subsequent extractions, with the first extract containing more than 90% of the total amount (as illustrated in Figure S6, Supporting Information). The mass of nitrate deposited in samples that had been exposed to NO under UV irradiation was in the range 150 – 480 µg. There was a non-negligible amount of nitrate present in the unexposed granules (75 – 105 µg), which was in all cases lower than the amount found in exposed granules. By contrast, very low levels of nitrite were observed, in the order of 1% of the nitrate mass. While nitrate results show good consistency between each pair of duplicate determinations, the nitrite data is much more scattered because reported levels were close to the limit of quantification.

The difference between NO-exposed and unexposed granules can be attributed to the formation of nitrate during the photocatalytic process. The amount of nitrate formed was compared with the predicted maximum mass calculated based on the NO_x deposited in a sample surface of 0.02 m^2. Overall, the amount of nitrate measured in the extracted samples was 42 – 69% of the predicted maximum nitrate mass for those samples. These quantities account for a large fraction of the expected nitrate recoveries in the extraction, but were below the predicted maximum values. This result is in line with a recent report by Mothes et al. [14], in which mass closure of nitrogenated species in a comparable experiment was achieved only when a relatively low amount of NO_x was removed (<25 µmol per m^2 of photocatalytic surface), and nitrate yields below 100% were observed when a higher amount of NO_x was removed. Our tests, with 75 – 325 µmol NO_x removed per m^2 of exposed granule surface, were comparable with the lower nitrate yield tests reported by Mothes et al. [14]. There are at least three possible explanations for the partial loss of nitrate in the extracted samples:

1) not all nitrate present in the material was extracted, with a fraction remaining strongly attached to the granules, possibly inside pores;
2) nitrate formed during the photocatalytic process may be partially adsorbed to chamber surfaces, and thus not extracted from the granules; and
3) other nitrogenated species, such as HNO_3, HONO or N_2O, may form during the photocatalytic process and be released to the gas phase [5, 32, 34].

Considering the very low levels of nitrite observed in the extracts, we do not expect high HONO concentrations in chamber air. Irreversible nitrate uptake in the bulk of granules and losses to reactor walls are likely the main reasons for the discrepancies between predicted and measured surface-bound nitrate. Even if low levels of HONO or N_2O were formed in the photocatalytic process, those contributions would likely be negligible compared with other naturally occurring sources of those species.

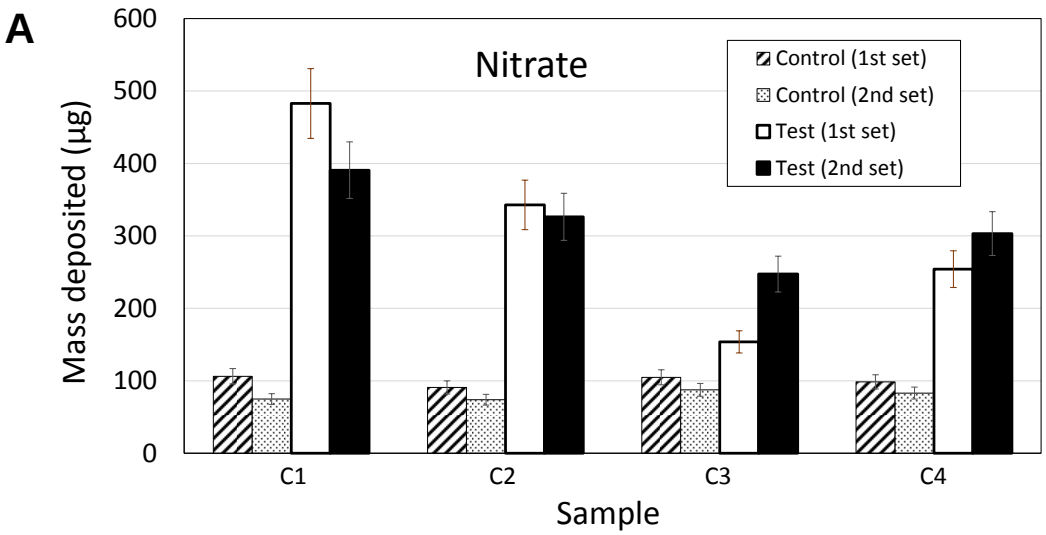

553

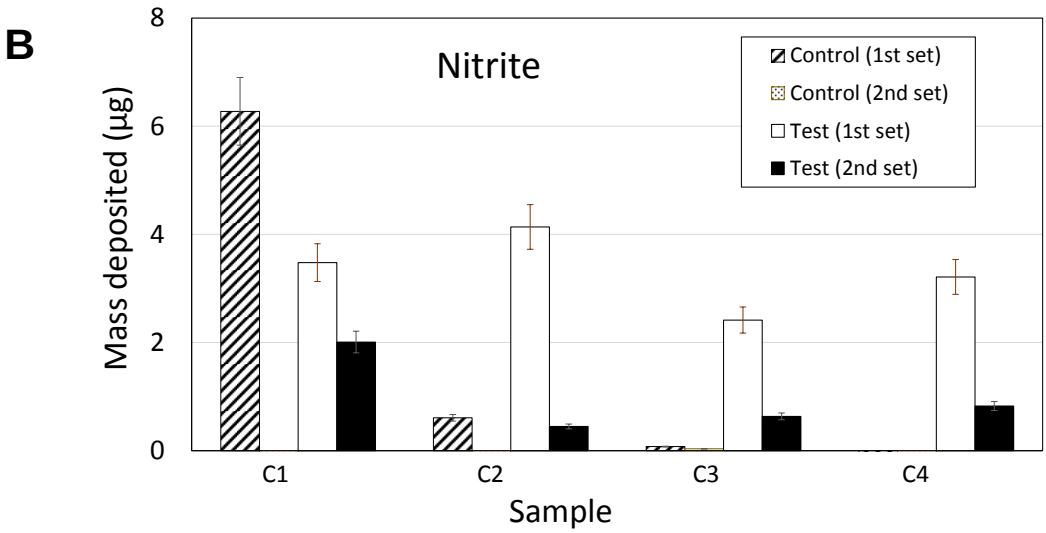

554

555

556

557 **Figure 8:** Mass of (A) nitrate and (B) nitrite ion determined in the first extraction of two sets of

558 loose granules.

559

4. Summary

The tested photocatalytic materials showed significant NO_x abatement activity, and can contribute to atmospheric de-noxification by oxidizing NO and NO_2 to adsorbed nitrate anions that can subsequently be washed away from the surface. Their performance was affected by key parameters such as the granule coating formulation, surface temperature and aging conditions.

Granule post-treatments applied over the TiO_2 coating, which are required to improve adhesion to the substrate, led to decreased photocatalytic performance. This study could not associate this partial inactivation to the presence of silicone in post-treatment formulations, despite suggestions to the contrary in the literature.

Evaluation of photocatalytic performance at room temperature, as specified by ISO Standard 22197-1, might underestimate the performance of building envelope materials, since their temperature is significantly higher under direct sunlight, and this study reports significantly better performance at 60 °C than at 25 °C. Variation of the ISO standard method using not only NO as the challenge gas but NO_2 or NO/ NO_2 mixture was also investigated, confirming the sensitivity of experimental results to the challenge gas composition.

The assessment of the effects of sample aging in the outdoor environment suggests potential performance enhancement by activation with solar irradiation and precipitation, as well as deactivation as a result of soiling, and possible catalyst inactivation. Experiments with specimens that were cleaned in the laboratory after environmental exposure showed also that the partial inactivation can be reversible.

This study provided only limited insight on the effect of aging, which is a function of location, climate and duration of exposure. A comprehensive testing plan spanning several years of exposure in multiple locations would be required to more completely assess aged performance.

Future work could advance this field by evaluating the performance of photocatalytic granulated roofing materials in large-scale demonstrations. Such studies could provide valuable insights on the impacts of the de-NO_x chemistry in the proximity of treated buildings, such as on street canyons where city dwellers are primarily exposed to urban pollution.

Acknowledgements

This research was funded by the Industrial Mineral Products Division of the 3M Company under contract FP00002421. Lawrence Berkeley National Laboratory operates under U.S. Department of Energy Contract DE-AC02-05CH11231.

References

[1] R.M. Levinson, S.S. Chen, G.A. Ban-Weiss, H.E. Gilbert, P.H. Berdahl, P.J. Rosado, H. Destaillats, M. Sleiman, T.W. Kirchstetter, Next-generation factory-produced cool asphalt shingles: Phase 1 final report, LBNL Report 2001007, (2016) Lawrence Berkeley National Laboratory, Berkeley, CA. http://escholarship.org/uc/item/2t3602nt.

[2] L. Picone, Asphalt low-sloped roofing: Enduring the test of time?, RCI Interface, September (2009) http://rci-online.org/wp-content/uploads/2009-2009-picone.pdf.

[3] M.R. Hoffmann, S.T. Martin, W.Y. Choi, D.W. Bahnemann, Environmental Applications Of Semiconductor Photocatalysis, Chem Rev, 95 (1995) 69-96. https://doi.org/ 10.1021/cr00033a004

[4] O. Carp, C.L. Huisman, A. Reller, Photoinduced reactivity of titanium dioxide, Prog Solid State Ch, 32 (2004) 33-177. https://doi.org/10.1016/j.progsolidstchem.2004.08.001

[5] S. Devahasdin, C. Fan Jr, K. Li, D.H. Chen, TiO_2 photocatalytic oxidation of nitric oxide: transient behavior and reaction kinetics, Journal of Photochemistry and Photobiology A: Chemistry, 156 (2003) 161-170. https://doi.org/10.1016/S1010-6030(03)00005-4

[6] S. Laufs, G. Burgeth, W. Duttlinger, R. Kurtenbach, M. Maban, C. Thomas, P. Wiesen, J. Kleffmann, Conversion of nitrogen oxides on commercial photocatalytic dispersion paints, Atmospheric Environment, 44 (2010) 2341-2349. http://doi.org/10.1016/j.atmosenv.2010.03.038

[7] J. Angelo, L. Andrade, A. Mendes, Highly active photocatalytic paint for NO_x abatement under real-outdoor conditions, Applied Catalysis A: General, 484 (2014) 17-25. http://dx.doi.org/10.1016/j.apcata.2014.07.005

[8] N. Bengtsson, M. Castellote, Photocatalytic Activity for NO Degradation by Construction Materials: Parametric Study and Multivariable Correlations, Journal of Advanced Oxidation Technologies, 13 (2010) 341-349. http://dx.doi.org/10.1515/jaots-2010-0311

[9] J.Z. Bloh, A. Folli, D.E. Macphee, Photocatalytic NO_x abatement: why the selectivity matters, RSC Advances, 4 (2014) 45726-45733. http://doi.org/10.1039/c4ra07916g

[10] A. Folli, C. Pade, T.B. Hansen, T. De Marco, D.E. Macphee, TiO_2 photocatalysis in cementitious systems: Insights into self-cleaning and depollution chemistry, Cement and Concrete Research, 42 (2012) 539-548. http://doi.org/10.1016/j.cemconres.2011.12.001

[11] M. Horgnies, I. Dubois-Brugger, E.M. Gartner, NO_x de-pollution by hardened concrete and the influence of activated charcoal additions, Cement and Concrete Research, 42 (2012) 1348-1355. http://doi.org/10.1016/j.cemconres.2012.06.007

[12] R. Sugranez, J.I. Alvarez, M. Cruz-Yusta, I. Marmol, J. Morales, J. Vila, L. Sanchez, Enhanced photocatalytic degradation of NO_x gases by regulating the microstructure of mortar cement modified with titanium dioxide, Building And Environment, 69 (2013) 55-63. http://dx.doi.org/10.1016/j.buildenv.2013.07.014

[13] L. Yang, A. Hakki, F. Wang, D.E. Macphee, Different roles of water in photocatalytic $DeNO_x$ mechanisms on TiO_2: Basis for engineering nitrate selectivity, ACS Appl. Mater. Interfaces, 9 (2017) 17034-17041. http://doi.org/10.1021/acsami.7b01989

[14] F. Mothes, S. Ifang, M. Gallus, B. Golly, A. Boreave, R. Kurtenbach, J. Kleffmann, C. George, H. Herrmann, Bed flow photoreactor experiments to assess the photocatalytic nitrogen oxides abatement under simulated atmospheric conditions, Applied Catalysis B: Environmental, 231 (2018) 161-172. http://doi.org/10.1016/j.apcatb.2018.03.010

[15] L. Yang, A. Hakki, F. Wang, D.E. Macphee, Photocatalyst efficiencies in concrete technology: The effect of photocatalyst placement, Applied Catalysis B: Environmental, 222 (2018) 200-208. http://doi.org/10.1016/j.apcatb.2017.10.013

[16] R. Zouzelka, J. Rathousky, Photocatalytic abatement of NO_x pollutants in the air using commercial functional coating with porous morphology, Applied Catalysis B: Environmental, 217 (2017) 466-476. http://dx.doi.org/10.1016/j.apcatb.2017.06.009

[17] M. Gallus, V. Akylas, F. Barmpas, A. Beeldens, E. Boonen, A. Boreave, M. Cazaunau, H. Chen, V. Daele, J.F. Doussin, Y. Dupart, C. Gaimoz, C. George, B. Grosselin, H. Herrmann, S. Ifang, R. Kurtenbach, M. Maille, A. Mellouki, K. Miet, F. Mothes, N. Moussiopoulos, L. Poulain, R. Rabe, P. Zapf, J. Kleffmann, Photocatalytic de-pollution in the Leopold II tunnel in Brussels: NO_x abatement results, Building And Environment, 84 (2015) 125-133. https://doi.org/10.1016/j.buildenv.2014.10.032

[18] M. Gallus, R. Ciuraru, F. Mothes, V. Akylas, F. Barmpas, A. Beeldens, F. Bernard, E. Boonen, A. Boreave, M. Cazaunau, N. Charbonnel, H. Chen, V. Daele, Y. Dupart, C. Gaimoz, B. Grosselin, H. Herrmann, S. Ifang, R. Kurtenbach, M. Maille, I. Marjanovic, V. Michoud, A. Mellouki, K. Miet, N. Moussiopoulos, L. Poulain, P. Zapf, C. George, J.F. Doussin, J. Kleffmann, Photocatalytic abatement results from a model street canyon, Environ. Sci. Pollut. Res., 22 (2015) 18185-18196. https://doi.org/10.1007/s11356-015-4926-4

[19] A. Folli, M. Strom, T.P. Madsen, T. Henriksen, J. Lang, J. Emenius, T. Klevebrant, A. Nilsson, Field study of air purifying paving elements containing TiO_2, Atmospheric Environment, 107 (2015) 44-51. http://dx.doi.org/10.1016/j.atmosenv.2015.02.025

[20] M.M. Ballari, H.J.H. Brouwers, Full scale demonstration of air-purifying pavement, J Hazard Mater, 254 (2013) 406-414. http://dx.doi.org/10.1016/j.jhazmat.2013.02.012

[21] E. Boonen, A. Beeldens, Recent Photocatalytic Applications for Air Purification in Belgium, Coatings, 4 (2014) 553-573. http://doi.org/10.3390/coatings4030553

[22] C.J. Cros, A.L. Terpeluk, L.E. Burris, N.E. Crain, R.L. Corsi, M.C.G. Juenger, Effect of weathering and traffic exposure on removal of nitrogen oxides by photocatalytic coatings on roadside concrete structures, Mater. Struct., 48 (2015) 3159-3171. http://doi.org/10.1617/s11527-014-0388-2

[23] C. George, A. Beeldens, F. Barmpas, J.F. Doussin, G. Manganelli, H. Herrmann, J. Kleffmann, A. Mellouki, Impact of photocatalytic remediation of pollutants on urban air quality, Front. Environ. Sci. Eng., 10(5) (2016) 1-11. http://doi.org/10.1007/s11783-016-0834-1

[24] M. Lettieri, D. Colangiuli, M. Masieri, A. Calia, Field performances of nanosized TiO_2 coated limestone for a self-cleaning building surface in an urban environment, Building and Environment, 147 (2019) 506-516. https://doi.org/10.1016/j.buildenv.2018.10.037

[25] K. Amrhein, D. Stephan, Principles and test methods for the determination of the activity of photocatalytic materials and their application to modified building materials, Photochem. Photobiol. Sci., 10 (2011) 338-342. http://doi.org/10.1039/c0pp00155d

[26] R. Dillert, J. Stotzner, A. Engel, D.W. Bahnemann, Influence of inlet concentration and light intensity on the photocatalytic oxidation of nitrogen(II) oxide at the surface of Aeroxide (R) TiO_2 P25, J Hazard Mater, 211 (2012) 240-246. http://doi.org/10.1016/j.jhazmat.2011.11.041

[27] A. Mills, C. Hill, P.K.J. Robertson, Overview of the current ISO tests for photocatalytic materials, J. Photochem. Photobiol. A-Chem., 237 (2012) 7-23. http://doi.org/10.1016/j.jphotochem.2012.02.024

[28] C. Minero, A. Bedini, M. Minella, On the Standardization of the Photocatalytic Gas/Solid Tests, International Journal of Chemical Reactor Engineering, 2013, pp. 717. https://doi.org/10.1515/ijcre-2012-0045

[29] ISO Standard 22197-1:2016, Fine ceramics (advanced ceramics, advanced technical ceramics) – test method for air-purification performance of semiconducting photocatalytic materials. , Part 1. Removal of nitric oxide. International Organization for Standardization, 2016. https://www.iso.org/standard/65416.html

[30] A. Mills, S. Elouali, The nitric oxide ISO photocatalytic reactor system: Measurement of NO_x removal activity and capacity, J. Photochem. Photobiol. A-Chem., 305 (2015) 29-36. http://doi.org/10.1016/j.jphotochem.2015.03.002

[31] S. Ifang, M. Gallus, S. Liedtke, R. Kurtenbach, P. Wiesen, J. Kleffmann, Standardization methods for testing photo-catalytic air remediation materials: Problems and solution, Atmospheric Environment, 91 (2014) 154-161. http://dx.doi.org/10.1016/j.atmosenv.2014.04.001

[32] S.K. Beaumont, R.J. Gustaftson, R.M. Lambert, Heterogeneous Photochemistry Relevant to the Troposphere: H_2O_2 Production during the Photochemical Reduction of NO_2 to HONO on UV-Illuminated TiO_2 Surfaces, Chemphyschem, 10 (2009) 331-333. http://doi.org/10.1002/cphc.200800613

[33] N. Bowering, G.S. Walker, P.G. Harrison, Photocatalytic decomposition and reduction reactions of nitric oxide over Degussa P25, Applied Catalysis B: Environmental, 62 (2006) 208-216. https://doi.org/10.1016/j.apcatb.2005.07.014

[34] R.J. Gustafsson, A. Orlov, P.T. Griffiths, R.A. Cox, R.M. Lambert, Reduction of NO2 to nitrous acid on illuminated titanium dioxide aerosol surfaces: implications for photocatalysis and atmospheric chemistry, Chemical Communications, (2006) 3936-3938. http://doi.org/10.1039/b609005b

[35] W. Lu, A.D. Olaitan, M.R. Brantley, B. Zekevat, D.A. Erdogan, E. Ozensoy, T. Solouki, Photocatalytic conversion of nitric oxide on titanium dioxide: Cryotrapping of reaction products for online monitoring by mass spectrometry, J. Phys. Chem. C, 120 (2016) 8056-8067. http://doi.org/10.1021/acs.jpcc.5b10631

[36] M. Ndour, B. D'Anna, C. George, O. Ka, Y. Balkanski, J. Kleffmann, K. Stemmler, M. Ammann, Photoenhanced uptake of NO2 on mineral dust: Laboratory experiments and model simulations, Geophysical Research Letters, 35 (2008). http://doi.org/10.1029/2007gl032006

[37] ASTM E1908-11. Standard Practice for Calculating Solar Reflectance Index of Horizontal and Low-Sloped Opaque Surfaces. ASTM International, West Conshohocken, PA, (2001), https://doi.org/10.1520/E1980-11.

[38] J.K. Sikkema, S.K. Ong, J.E. Alleman, Photocatalytic concrete pavements: Laboratory investigation of NO oxidation rate under varied environmental conditions, Construction and Building Materials, 100 (2015) 305-314. http://dx.doi.org/10.1016/j.conbuildmat.2015.10.005

716 [39] C.J. Cros, A.L. Terpeluk, N.E. Crain, M.C.G. Juenger, R.L. Corsi, Influence of environmental
717 factors on removal of oxides of nitrogen by a photocatalytic coating, Journal of the Air & Waste
718 Management Association, 65 (2015) 937-947. http://dx.doi.org/10.1080/10962247.2015.1040524

719 [40] F. Bai, R.A.T. Gould, M.T.M. Anderson, Photocatalytic coating, US Patent, 8,993,471 B2
720 (2015) https://patents.google.com/patent/US8993471B8993472/en.

721 [41] J.L.M. Jacobs, Photocatalytic composition and method for preventing algae growth on
722 building materials, US Patent, 6,881,701 B2 (2005) https://patents.google.com/patent/US6881701.

723 [42] ASTM G154-12a. Standard practice for operating fluorescent ultraviolet (UV) lamp apparatus
724 for exposure of nonmetallic materials. ASTM International, West Conshohocken, PA. (2012).
725 https://doi.org/10.1520/G0154-12A.

726 [43] Q-Lab, Q-Lab weathering research service. Florida - Arizona - Natural - Accelerated,
727 https://www.q-lab.com/documents/public/a22e6272-737d-4e26-9bd9-d0ecc0bc2c20.pdf, (2008).

728 [44] L. Sivachandiran, F. Thevenet, P. Gravejat, A. Rousseau, Investigation of NO and NO2
729 adsorption mechanisms on TiO_2 at room temperature, Applied Catalysis B: Environmental, 142-
730 143 (2013) 196-204. http://doi.org/10.1016/j.apcatb.2013.04.073

731 [45] M. Ndour, P. Conchon, B. D'Anna, O. Ka, C. George, Photochemistry of mineral dust surface
732 as a potential atmospheric renoxification process, Geophysical Research Letters, 36 (2009)
733 L05816. http://doi.org/10.1029/2008GL036662

734 [46] O. Rosseler, M. Sleiman, V.N. Montesinos, A. Shavorskiy, V. Keller, N. Keller, M.I. Litter,
735 H. Bluhm, M. Salmeron, H. Destaillats, Chemistry of NO_x on TiO_2 surfaces studied by ambient
736 pressure XPS: products, effect of UV irradiation, water, and coadsorbed K^+, J. Phys. Chem. Lett.,
737 4 (2013) 536-541. http://doi.org/10.1021/jz302119g

738 [47] L. Sivachandiran, F. Thevenet, A. Rousseau, D. Bianchi, NO_2 adsorption mechanism on TiO_2:
739 An in-situ transmission infrared spectroscopy study, Applied Catalysis B: Environmental, 198
740 (2016) 411-419. http://dx.doi.org/10.1016/j.apcatb.2016.05.065

741 [48] L. Cao, Z. Gao, S.L. Suib, T.N. Obee, S.O. Hay, J.D. Freihaut, Photocatalytic Oxidation of
742 Toluene on Nanoscale TiO_2 Catalysts: Studies of Deactivation and Regeneration, Journal of
743 Catalysis, 196 (2000) 253-261. https://doi.org/10.1006/jcat.2000.3050

744 [49] M.K. Chemweno, L.G. Cernohlavek, W.A. Jacoby, Deactivation of titanium dioxide
745 photocatalyst by oxidation of polydimethylsiloxane and silicon sealant off-gas in a recirculating
746 batch reactor, J. Air & Waste Manag. Assoc., 58 (2008) 12-18. http://dx.doi.org/10.3155/1047-
747 3289.58.1.12

748 [50] S.O. Hay, T.N. Obee, C. Thibaud-Erkey, The deactivation of photocatalytic based air purifiers
749 by ambient siloxanes, Applied Catalysis B: Environmental, 99 (2010) 435-441.
750 http://doi.org/10.1016/j.apcatb.2010.06.018

751

SUPPORTING INFORMATION

De-pollution efficacy of photocatalytic roofing granules

Xiaochen Tang[1], Lara Ughetta[2], Simon K. Shannon[2], Sébastien Houzé de l'Aulnoit[1], Sharon Chen[1], Rachael A. T. Gould[2], Marion L. Russell[1], Jiachen Zhang[3], George Ban-Weiss[3], Rebecca L. A. Everman[2], Frank W. Klink[2], Ronnen Levinson[1], Hugo Destaillats[1,*]

1. Heat Island Group, Lawrence Berkeley National Laboratory, 1 Cyclotron Road, Berkeley, California 94720.
2. Industrial Mineral Products Division, The 3M Company, 3M Center, Building 209, 01-W-14, St. Paul, Minnesota 55144.
3. Department of Civil and Environmental Engineering, University of Southern California, Los Angeles, California 90089, USA.

* Corresponding author E-mail: HDestaillats@lbl.gov

Note S1: Broadband UV irradiance from UVA-340 lamp in weathering apparatus

The broadband UV irradiance (also known as “total ultraviolet”, or TUV) delivered by the UVA-340 lamp in the commercial weathering apparatus (Model QUV/Spray with Solar Eye Irradiance Control, Q-Lab) when operated in accordance with Cycle 1 of ASTM Standard G154-12a “Standard Practice for Operating Fluorescent Ultraviolet (UV) Lamp Apparatus for Exposure of Nonmetallic Materials” [1] was computed by

a. digitizing the spectral irradiance labeled “UVA-340” in Figure 11 of Q-Lab Technical Bulletin LU-0822 “Sunlight, Weathering & Light Stability Testing”; [2]
b. scaling this spectral irradiance to attain the value of 0.89 W m^{-2} nm^{-1} at 340 nm specified by ASTM G154-12a, Cycle 1; and
c. integrating the scaled irradiance from 295 to 400 nm.

The resulting broadband UV irradiance was 48.0 W m^{-2}, or 173 kJ m^{-2} per hour of lamp operation. Note that the lamp is on 8 h and off 4 h in each 12-h cycle.

[1] ASTM G154-12a, Standard practice for operating fluorescent ultraviolet (UV) lamp apparatus for exposure of nonmetallic materials, ASTM International, West Conshohocken, PA, 2012. https://doi.org/10.1520/G0154-12A

[2] Technical Bulletin LU-0822, Sunlight, weathering & light stability testing. Q-Lab Corporation, Westlake, OH, 2011. https://www.q-lab.com/documents/public/cd131122-c252-4142-86ce-5ba366a12759.pdf

Table S1: Solar reflectance of shingle prototypes (Group A).

Sample ID	Average	Standard Deviation
A0	0.225	0.010
A1	0.167	0.006
A2	0.163	0.003
A3	0.118	0.007
A4	0.299	0.003
A5	0.287	0.006

The values reported in Table S1 represent the average of three measurements per specimen following ASTM C1549-16 “Standard Test Method for Determination of Solar Reflectance Near Ambient Temperature Using a Portable Solar Reflectometer”.[3] We used a Solar Spectrum Reflectometer (Devices & Services; Dallas, Texas, version 6) with the air mass 1.5 beam-normal solar reflectance output “1.5E”, as specified by the ANSI/CRRC-1-2016 Standard.[4]

[3] ASTM C1549-16, Standard test method for determination of solar reflectance near ambient temperature using a portable solar reflectometer. ASTM International, West Conshohocken, PA, 2016. https://doi.org/10.1520/C1549-16

[4] ANSI/CRRC-1-2016 Standard test methods for determining radiative properties of materials. American National Standards Institute / Cool Roof Rating Council, 2016. http://coolroofs.org/product-rating/ansi-crrc-s100

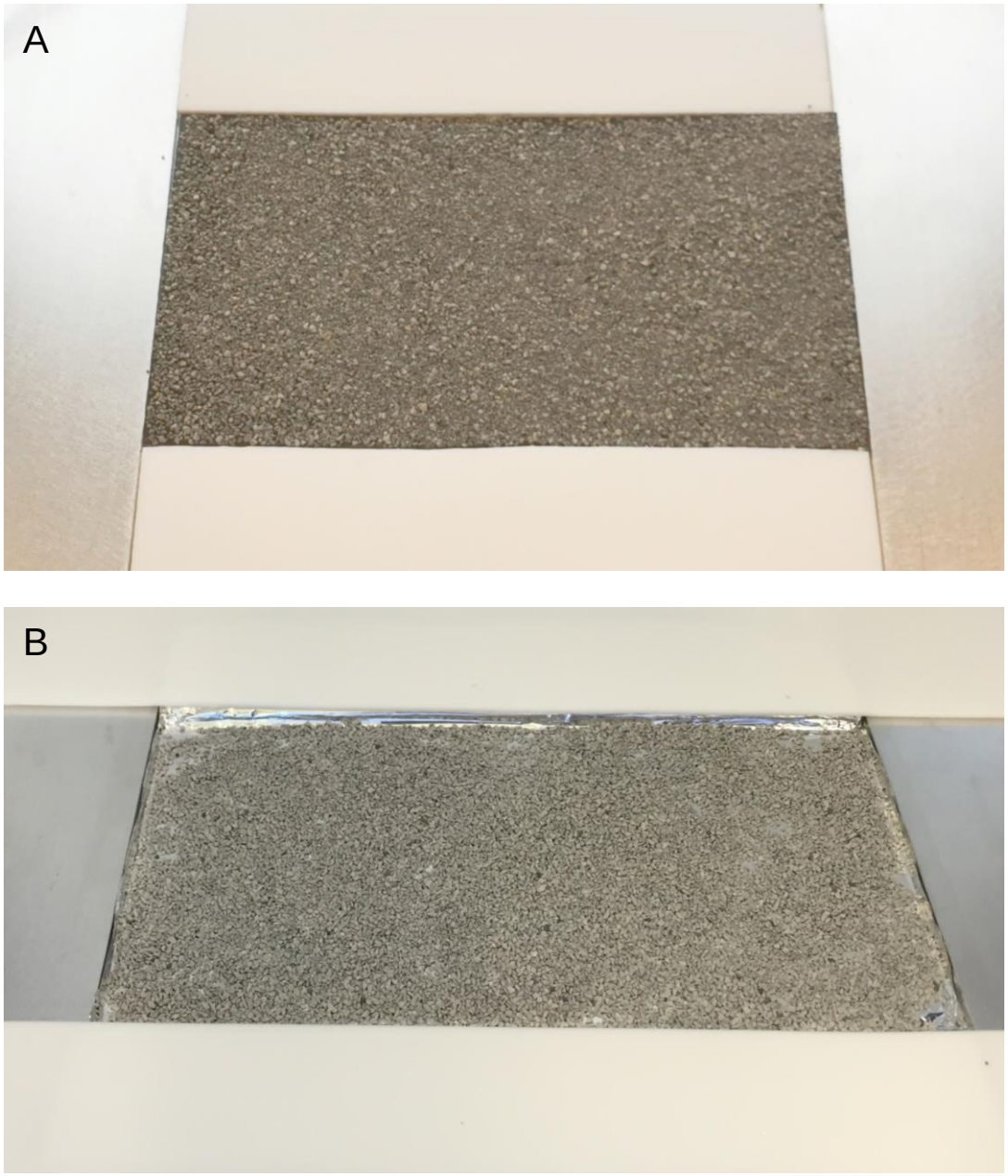

Figure S1: (A) Shingle specimen and (B) loose granules spread evenly inside the exposure chamber.

Figure S2: Rack used for natural exposure in Berkeley, CA.

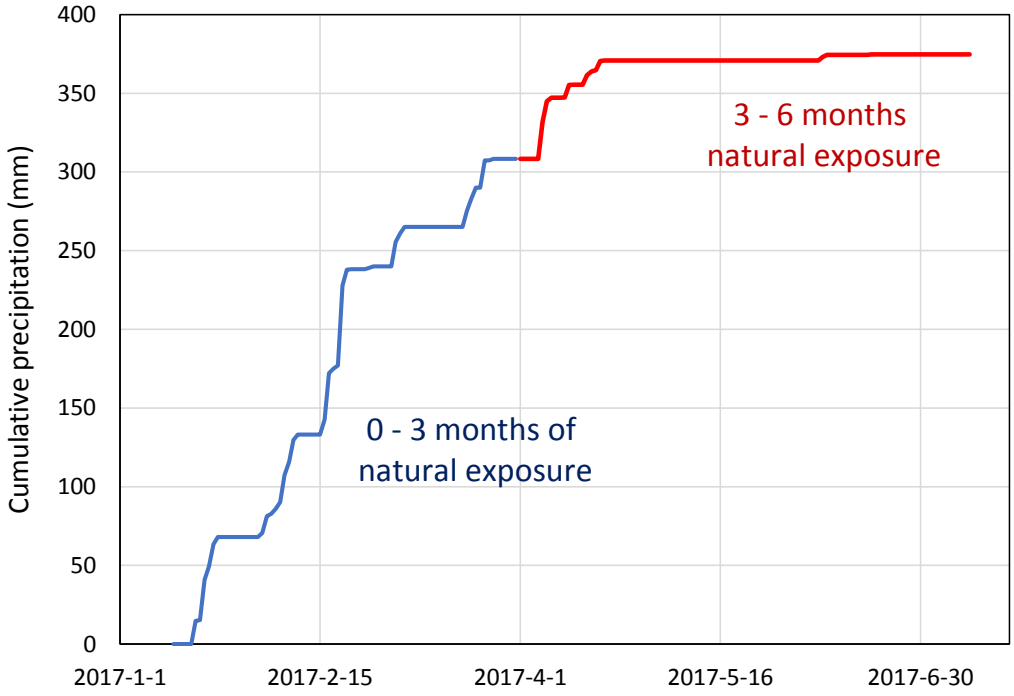

Figure S3: Cumulative precipitation in Berkeley, CA, during the six-month exposure period for samples A4 and A5.

Table S2: Hourly average solar irradiance (W m^{-2}) measured at the California Irrigation Management Information System (CIMIS) Station 213 in El Cerrito, CA.

Hour of day*	Average solar irradiance 2016-03-25 to 2016-07-11	Average solar irradiance 2017-01-13 to 2017-07-11
1	0	0
2	0	0
3	0	0
4	0	0
5	0.6	0.3
6	17	8.6
7	118	69
8	267	164
9	424	291
10	577	405
11	718	496
12	798	547
13	831	559
14	796	544
15	705	472
16	563	374
17	389	251
18	212	127
19	65	39
20	3.4	2.1
21	0	0
22	0	0
23	0	0
24	0	0

* For example, hour of day 1 = 0:00 - 1:00.

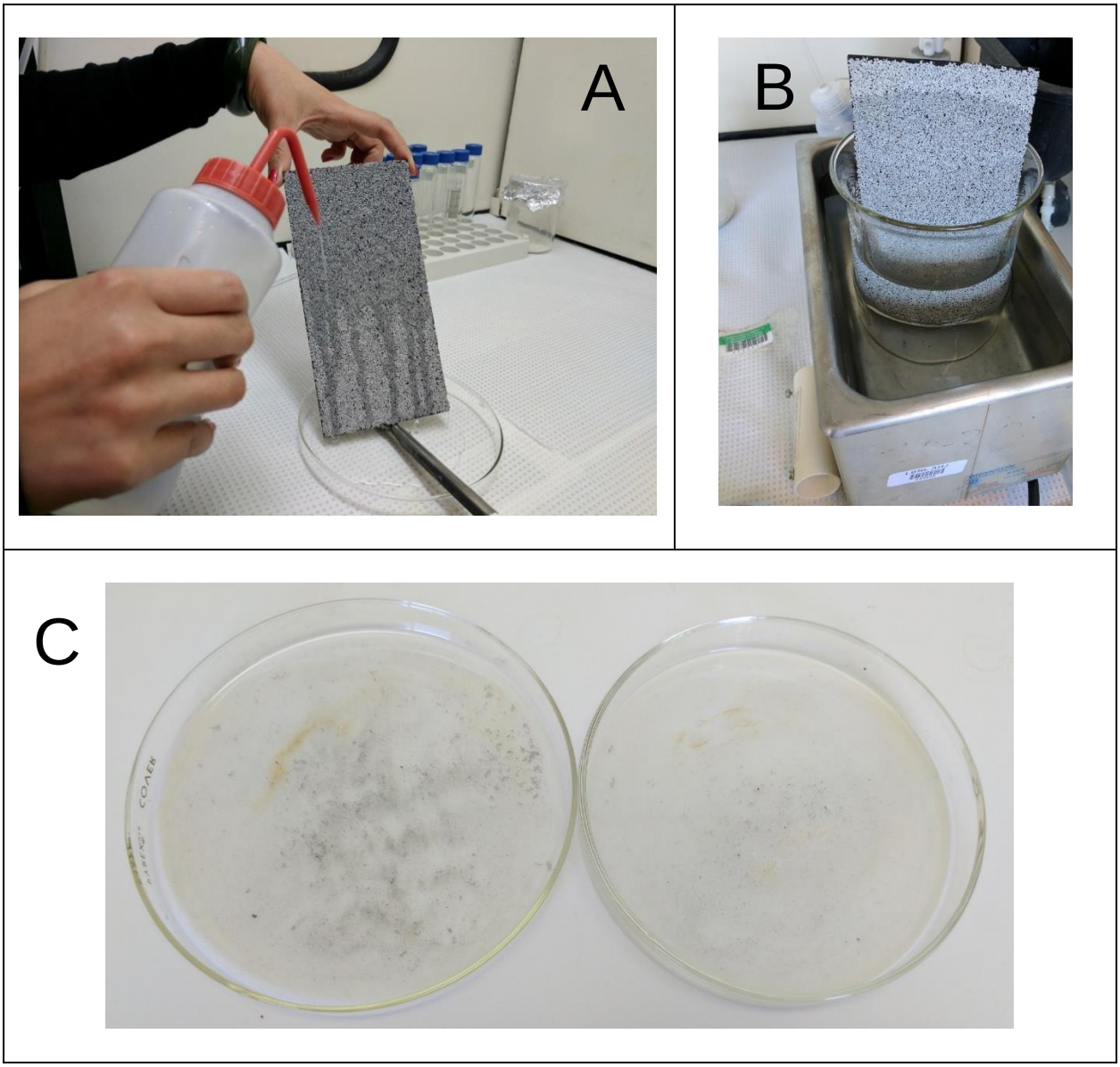

Figure S4: Laboratory cleaning operations applied to A4 and A5 specimens exposed for six months in Berkeley, CA. Images show (A) “soft cleaning” by rinsing; (B) “hard cleaning” using sonication; and (C) residues collected on petri dish during “soft cleaning”.

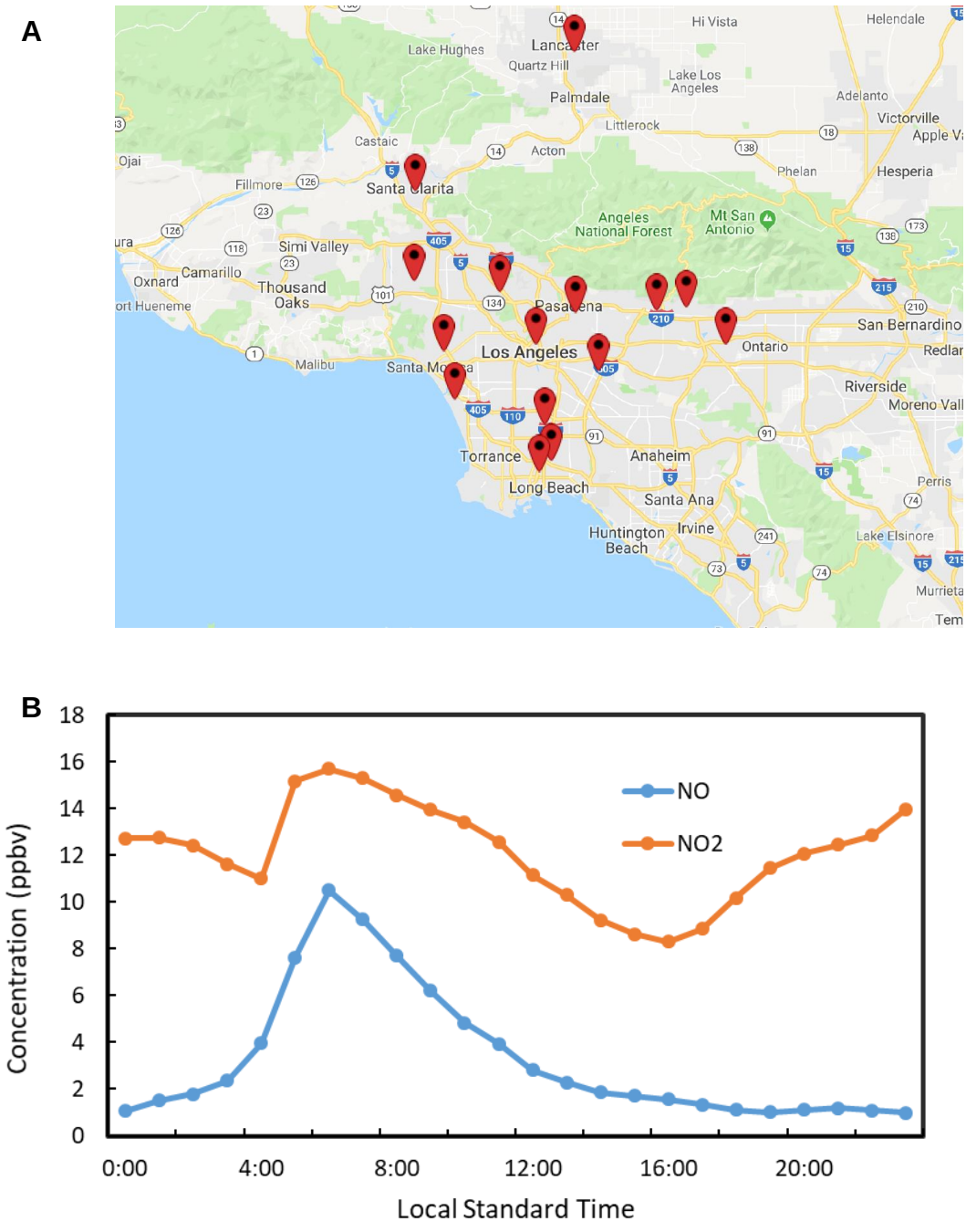

Figure S5: Evaluation of NO/NO_2 mixing ratio in Los Angeles. (A) Map showing the 13 stations monitoring NO and NO_2 in Los Angeles County; (B) Diurnal cycles of NO and NO_2 concentrations averaged among the 13 monitoring stations in Los Angeles County for July 2012.

Records corresponding to NO and NO_2 concentrations for 13 monitoring stations in Los Angeles County were obtained from the EPA Air Quality System (AQS).[5] AQS data are collected from local, state, and federal air quality control agencies. Figure S5-A shows the location of the stations used in our analysis. Figure S5-B shows the diurnal cycles of NO and NO_2 concentrations averaged over the stations in Los Angeles County for July 2012.

As shown in Table S3, the ratio of daytime (06:00 – 20:00 local standard time [LST]) average NO to NO_2 concentrations is calculated to be 0.29 (~0.3).

[5] US Environmental Protection Agency (US EPA). Air Quality System (AQS), 2018. https://www.epa.gov/aqs

Table S3. Average, maximum, and minimum values of NO and NO_2 concentrations and the ratio of hourly NO to NO_2 concentrations during daytime (06:00 – 20:00 LST). Values were averaged among 13 AQS monitoring stations (shown in Figure S4-A) in Los Angeles County for July 2012.

	NO (ppb)	**NO_2 (ppb)**	**NO/NO_2 ratio**
Average	3.8	11.7	0.29
Maximum	10.5	15.7	0.67
Minimum	1.0	8.3	0.09

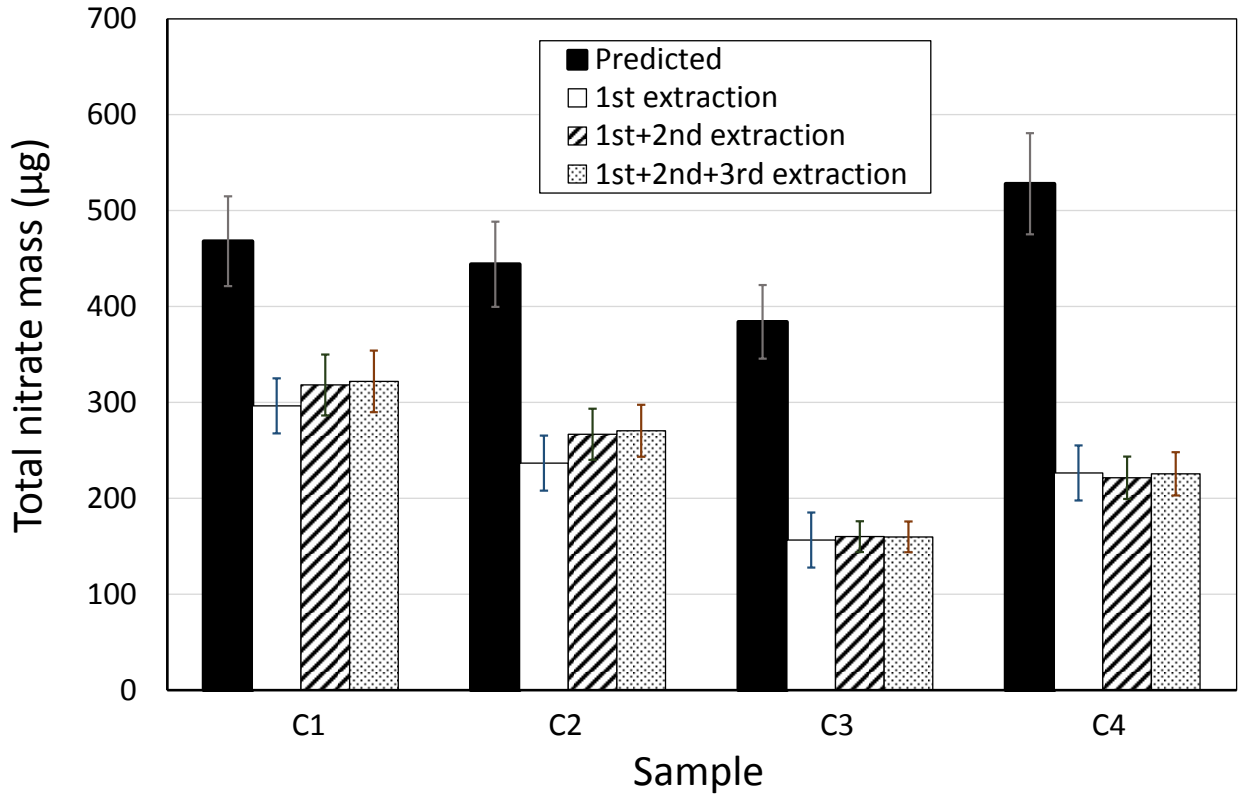

Figure S6: Comparison of the predicted mass of nitrate formed during the photocatalytic process and the amounts recovered with one, two and three sequential extraction of exposed granules.